Driven dynamics of a quantum dot electron spin coupled to a bath of higher-spin nuclei

Arian Vezvaee, Girish Sharma, Sophia E. Economou, and Edwin Barnes

Phys. Rev. B **103**, 235301 — Published 1 June 2021

DOI: 10.1103/PhysRevB.103.235301

Driven dynamics of a quantum dot electron spin coupled to bath of higher-spin nuclei

Arian Vezvaee[1],* Girish Sharma[2], Sophia E. Economou[1], and Edwin Barnes[1]†
[1]*Department of Physics, Virginia Tech, Blacksburg, Virginia 24061, USA*
[2]*School of Basic Sciences, Indian Institute of Technology Mandi, India*

The interplay of optical driving and hyperfine interaction between an electron confined in a quantum dot and its surrounding nuclear spin environment produces a range of interesting physics stemming from the creation of dynamic nuclear polarization. In this work, we go beyond the ubiquitous spin 1/2 approximation for nuclear spins and present a comprehensive theoretical framework for an optically driven electron spin in a self-assembled quantum dot coupled to a nuclear spin bath of arbitrary spin. Using a dynamical mean-field approach, we compute the nuclear spin polarization distribution with and without the quadrupolar coupling. We find that while hyperfine interactions drive dynamic nuclear polarization in such a way that the electron spin precession becomes synchronized with the driving, quadrupolar couplings counteract this phenomenon. The tension between these mechanisms is imprinted on the steady-state electron spin evolution, providing a way to measure the importance of quadrupolar interactions in a quantum dot. Our results show that higher-spin effects such as quadrupolar interactions can have a significant impact on the generation of dynamic nuclear polarization and how it influences the electron spin evolution.

I. INTRODUCTION

Spins in self-assembled quantum dots (QDs) are under intense investigation for a variety of quantum information applications, including quantum information processing, quantum communication, and quantum transduction [1–4]. The relatively long coherence times, fast controllability [5–7], and good photon emission properties of these systems [8–11] make them promising candidates for achieving high-quality spin-photon interfaces and for producing large-scale multi-photon entangled states [12–15]. The deterministic generation of these multi-photon entangled states has been demonstrated experimentally using the dark excitonic states of QDs [16].

While optically controlled quantum dot spins offer a wide range of technological possibilities, hyperfine (HF) interactions between the confined spin and its surrounding nuclear spin bath have been a major impediment. This interaction is the main source of decoherence in these systems, and it also causes spectral wandering and inhomogeneities in quantum dot ensembles, aspects that have been researched extensively over the past two decades [17–51]. However, many works have shown that the state of the bath, and consequently its deleterious effects, can be influenced by driving the electron spin. For example, several experiments have shown that driving can generate dynamic nuclear polarization (DNP), an effect that has been observed in self-assembled QDs [52–64] and also in other systems such as gated QDs [65–68], quantum wires [69] and in bulk materials [70, 71], findings that have been supported by a number of theory works [72–84]. In self-assembled QDs, it has been shown that DNP can survive on the order of minutes due to the suppression of nuclear spin diffusion caused by strain-induced quadrupolar interactions [85–87]. An important example of DNP in self-assembled QDs is the mode-locking experiments of Refs. [52–58], where an ensemble of QD electron spins becomes synchronized with a periodic train of optical pulses as a consequence of DNP. Continuous-wave laser driving of the electron has been shown to create DNP in QDs as well, leading to interesting phenomena such as the line-dragging effect, i.e. the locking of an optical QD transition to the frequency of the laser [60, 62, 63, 76, 88]. Owing to the long coherence times of nuclear spins, DNP has been proposed for applications such as quantum memories [89, 90], which has recently been demonstrated experimentally [91, 92].

Although most of the fully quantum mechanical theoretical treatments of the hyperfine decoherence problem allow for nuclei with spin greater than 1/2 [22–24], studies of the driven, hyperfine-induced generation of DNP have mostly focused on spin 1/2 nuclei to reduce the computational complexity of the problem [53, 72, 73, 81, 82, 93]. The latter works typically rely on either stochastic equations or rate equations to solve for the nuclear polarization distribution. While solving the feedback problem for spin 1/2 nuclear baths can yield qualitative insights about DNP experiments, the quantitative accuracy of such models is limited by the fact that the most commonly studied semiconductor QDs are in materials such as InAs or GaAs, which contain nuclei of spin $I > 1/2$. In addition to artificially reducing the size of the bath Hilbert space, assuming spin 1/2 nuclei also ignores effects such as quadrupolar interactions, which are only present for $I > 1/2$. There do exist a few theoretical works that allow for $I > 1/2$ [18, 37, 74]. Specifically, Huang and Hu [18] studied DNP arising from hyperfine interactions with the spin 3/2 arsenic nuclei in InGaAs by making use of Fermi's golden rule; however, only qualitative agreement with experiment was achieved due to the need to introduce phenomenological parameters. Yang and Sham [74] presented a general framework for nuclei of arbitrary total spin by unifying the stochas-

* avezva@vt.edu
† efbarnes@vt.edu

tic and rate-equation approaches. In this work they focused on a drift feedback loop (which allows for a possible bias in nuclear spin-flip processes) and obtained a Fokker-Planck equation for the polarization of the bath. Although this framework captures line-dragging and other DNP phenomena seen in experiments, it has only been established for continuous-wave driving, and so it is not immediately applicable to experiments with periodic driving such as the mode-locking experiments of Refs. [52–58]. Theoretical works that have specifically focused on mode-locking type experiments have either assumed $I = 1/2$ nuclear baths [72, 73] or utilized semiclassical methods [94–100]. While semiclassical approaches have been successful in reproducing qualitative features seen in experiments including dynamic nuclear polarization and mode-locking, it remains an outstanding challenge to develop a more quantitatively accurate description of the driven electron-nuclear spin system. Unlike in the case of nuclear-spin-induced decoherence, where semiclassical treatments have been shown to agree well with quantum mechanical ones [79, 101–103], similar comparisons in the context of optically driven DNP have revealed significant quantitative differences [95].

In this paper, we develop a quantum, non-perturbative framework to solve the dynamics of an optically driven electron spin coupled to a bath of $I > 1/2$ nuclear spins. We focus on DNP feedback mechanisms that arise from driving the electron with a periodic train of optical pulses while it is subject to hyperfine interactions with a nuclear spin bath, as in the mode-locking experiments [52–58]. Here, we also consider the effect of quadrupolar interactions. To compute DNP and its effect on the evolution of the electron spin, we use an approach based on dynamical maps and kinetic equations introduced in Refs. [72, 73], but, importantly, here we generalize the formalism to higher nuclear spin and treat the problem non-perturbatively, unlike in these earlier works. Our framework provides a self-consistent description of the feedback loop between the driven electron and DNP.

We compute the nuclear spin polarization distribution and its influence on the electron spin evolution for spin 1 and spin 3/2 baths and compare the results to the $I = 1/2$ case. Our approach is able to treat bath sizes of up to thousands of nuclear spins in the $I = 1/2$ and $I = 1$ cases, and up to several hundred spins in the $I = 3/2$ case. Although evidence of mode-locking is seen in all three cases, we find that quadrupolar interactions act to suppress mode-locking for $I > 1/2$, especially when the angle between the principal strain axis and the applied magnetic field is large. We also find that while HF interactions can produce a significant bath polarization that grows linearly with the number of nuclei for $I > 1/2$, quadrupolar interactions work to counteract this buildup of DNP. We further show that the relative importance of quadrupolar effects grows as the magnitude of the applied magnetic field is increased. The competition between HF and quadrupolar interactions imprints clear signatures in the steady-state electron spin evolution, providing an experimental tool to measure the strength of quadrupolar couplings in a QD. Our results show that accounting for higher nuclear spin is important not only for quantitative accuracy, but also for capturing important qualitative features of the DNP process in driven QD systems.

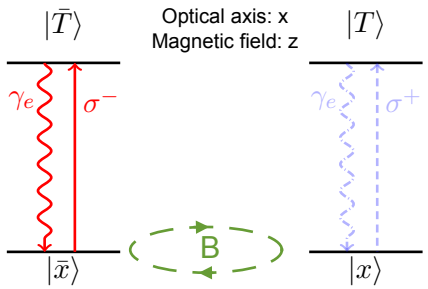

FIG. 1. The relevant level structure in the mode-locking experiments. $|x\rangle$ and $|\bar{x}\rangle$ are the electron spin states along the optical axis. These states are coupled by an external magnetic field along the z direction. Circularly polarized light excites the ground electron spin states to excited trion levels $|T\rangle$ and $|\bar{T}\rangle$ with angular momentum projections $+3/2$ and $-3/2$, respectively. The selection rules are such that each ground state couples to only one excited state. The trion states decay via spontaneous emission with rate γ_e. In this work, we focus on left-circularly polarized driving.

The paper is structured as follows. In Sec. II, we describe the system and Hamiltonian. In Sec. III, we lay out the theoretical approach in detail for arbitrary nuclear spin I and construct the equations that govern DNP for $I = 1/2$, 1, and 3/2 nuclear spin baths. We present an analytical solution for the steady-state nuclear spin polarization distribution for $I = 1/2$. In Sec. IV, we numerically compute steady-state polarization distributions for $I = 1$ and 3/2 and compare the results to the $I = 1/2$ solution for various parameter choices. We also study the effect of DNP on the electron spin evolution. We conclude in Sec. V. Two appendices contain details about the steady state of a driven electron spin in the absence of HF interactions.

II. SYSTEM AND HAMILTONIAN

Our focus in this work is on QD experiments in which a single electron is periodically pumped by a train of optical pulses [52–58, 104]. Each pulse excites the electron to a trion state (a bound state of an electron and an exciton), which then decays back to the electronic ground state manifold via spontaneous emission. The full Hamiltonian of the nuclear spin bath and the driven electron is given by

$$H(t) = H_{0,e} + H_{0,n} + H_c(t) + H_{res} + H_{HF} + H_Q. \quad (1)$$

Here, $H_{0,e}$ describes the electronic degrees of freedom in the QD in the absence of driving:

$$H_{e,0} = \omega_e \hat{S}_z + \omega_{\bar{T}} |\bar{T}\rangle\langle\bar{T}|, \quad (2)$$

where ω_e is the electron spin Zeeman frequency, $\hat{S}_z$ is the spin operator in the electronic ground space, and $\omega_{\bar{T}}$ is the energy of the trion state $|\bar{T}\rangle$. We take the magnetic field to be oriented along the z direction, while the optical axis lies in the x direction (see Fig. 1). We neglect the second trion level $|T\rangle$ in $H_{0,e}$ because it is not excited by the laser polarization we are considering. This driving is described by the Hamiltonian

$$H_c(t) = \Omega(t)|\bar{x}\rangle\langle\bar{T}| + h.c., \tag{3}$$

where we assume the drive laser is left-circularly polarized (red arrow in Fig. 1) with periodic temporal profile $\Omega(t+T_R) = \Omega(t)$, so that each pulse couples the electron spin state $|\bar{x}\rangle$ to the trion state $|\bar{T}\rangle$. The latter decays via spontaneous emission with rate γ_e. This process arises from interactions with a photonic bath, which is represented by the term H_{res}. We do not give an explicit expression for this term as it is not needed in what follows. The Zeeman splitting of the nuclear spins is given by $H_{0,n} = \omega_n \sum_i \hat{I}^i_z$.

The HF interaction is given by the contact term:

$$H_{HF} = \sum_{i=1}^{N} A_i \hat{S}_z \hat{I}^i_z + \sum_{i=1}^{N} A_i/2(\hat{S}_+\hat{I}^i_- + \hat{S}_-\hat{I}^i_+), \tag{4}$$

where N is the number of nuclei that interact appreciably with the electron. The first term is referred to as the Overhauser term, and it gives rise to an effective magnetic field seen by the electron spin in the case of nonzero nuclear spin polarization. The second term generates flip-flop interactions under which the electron spin flips with a nuclear spin. These terms are responsible for transferring angular momentum from the electron onto the nuclei, while the Overhauser term is the primary mechanism for feedback between the nuclear spin polarization and the electron spin evolution. The HF couplings A_i are determined by the magnitude of the electronic wave function at the location of the nuclear spin I^i. However, on timescales short compared to $N/\mathcal{A} \sim \mu$s, where $\mathcal{A}$ is the total HF interaction energy, the variations in these couplings do not significantly affect the electron spin evolution [105]. Here, we focus on fast optical driving where the electron reaches a steady state over a timescale of about 100 ns [73], which allows us to make the "box model" approximation in which all the HF couplings are taken equal: $A_i = A \equiv \mathcal{A}/N$ [105, 106]. Further comments about this approximation are given in Sec. V.

The quadrupolar interaction is given by [107, 108]

$$H_Q = \sum_{i=1}^{N} \frac{\nu^i_Q}{2}\left(\hat{I}^{i\,2}_{z'} - \frac{I(I+1)}{3}\right). \tag{5}$$

This interaction occurs due to the coupling of the nuclear quadrupole moment to electric field gradients caused by strain in the semiconductor lattice, and it is only present for $I > 1/2$. The presence of quadrupolar interactions has lead to striking phenomena in various types of experiments conducted in QDs. A few examples include the anomalous Hanle effect [43] and suppression of spin diffusion [41]. Line-dragging phenomena have also been associated with the presence of quadrupolar interactions [62, 63, 74]. The coupling strength ν_Q is referred to as the nuclear quadrupole resonance frequency, which is estimated to be around 2.8 MHz for As [41]. The quadrupole resonance frequency generally depends on the local strain in the vicinity of each nuclear spin, and so it generally varies across the material. Here, we assume that the strain remains roughly constant over the QD, and so we take all the frequencies to be equal: $\nu^i_Q = \nu_Q$. The operator $\hat{I}_{z'}$ in Eq. (5) is the component of the nuclear spin operator along the principal axis of the electric field gradient. Our focus will be on the case of QDs with cylindrical symmetry in which the electric field gradient makes an angle θ with the magnetic field. Therefore, we have $\hat{I}_{z'} = \hat{I}_z\cos\theta + \hat{I}_x\sin\theta$, which then gives [107]:

$$H_Q = \frac{\nu_Q}{2}\sum_{i=1}^{N}\Big[(\hat{I}^i_z)^2\cos^2\theta - \frac{I(I+1)}{3} + (\hat{I}^i_z\hat{I}^i_x + \hat{I}^i_x\hat{I}^i_z)\sin\theta\cos\theta + (\hat{I}^i_x)^2\sin^2\theta\Big]. \tag{6}$$

When $\theta = 0$, H_Q creates non-uniform energy spacings between the nuclear spin levels. For $\theta \neq 0$, H_Q has the additional effect of driving $\Delta m_I = \pm 1$ and $\Delta m_I = \pm 2$ nuclear spin-flip transitions, where m_I is the eigenvalue of $\hat{I}_z$. Notice that the rate for $\Delta m_I = \pm 1$ transitions is maximal at $\theta = \pi/4$, while the rate for $\Delta m_I = \pm 2$ transitions is largest for $\theta = \pi/2$, which is also the value of θ where the non-uniformity in the energy level spacings is zero. Thus, we see that the role of H_Q changes as θ varies from 0 to $\pi/4$, and from $\pi/4$ to $\pi/2$. Because H_Q is π-periodic in θ, it suffices to focus on the range $0 \leq \theta \leq \pi/2$.

In the case of $I = 1/2$ nuclei, the underlying physical mechanism behind the formation of DNP can be understood as follows. Imagine that the electron spin starts in a pure (polarized) state and the nuclear spins are in a totally mixed (unpolarized) state. The HF interaction then transfers angular momentum from the electron onto the nuclei, creating DNP. In the absence of driving, this would lead to only a modest nuclear spin polarization, and this polarization would be short-lived because it would eventually be transferred back to the electron via the HF interaction. However, the laser pulses periodically reset the electron spin to a polarized state, enabling a net transfer of angular momentum from the laser, through the electron, and onto the nuclei. This basic mechanism can also underlie DNP in nuclear spin baths with $I > 1/2$, however it is unclear what role the quadrupolar interactions play in this story. Answering this question is a main goal of this work.

It is worth noting that our Hamiltonian, Eq. (1), does not include inter-nuclear dipolar interactions. In self-assembled QDs, these interactions are weak compared to the hyperfine and quadrupolar interactions, and their

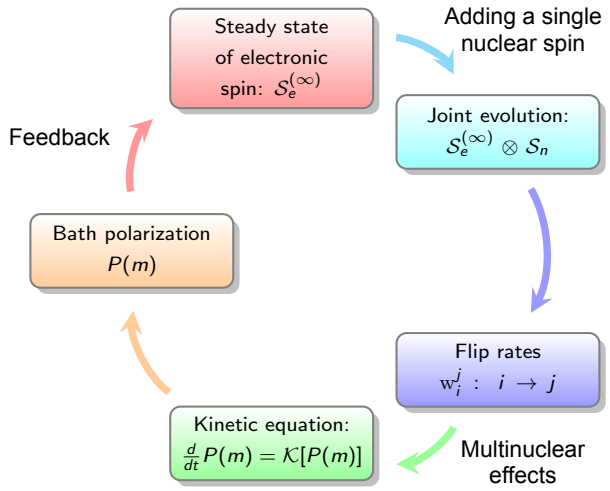

FIG. 2. Schematic depiction of the self-consistent formalism we use to model DNP with feedback. We exploit a hierarchy of timescales to first solve for the joint evolution of the electron coupled to a single nuclear spin. Under a Markovian approximation, the electron spin state is reset after each drive period. The resulting nuclear spin evolution yields nuclear spin-flip rates that are then fed into a kinetic equation governing the dynamics of the multi-nuclear spin polarization distribution. The flip rates depend on the effective electron spin precession frequency, including the Overhauser field contribution for self-consistency. The solution to the kinetic equation is then used to update the electron steady state, closing the feedback loop.

main effect is to drive nuclear spin diffusion, which gradually causes the decay of DNP. It has been shown experimentally, however, that this diffusion process is strongly suppressed in self-assembled QDs due to strain [85–87], leading to diffusion times in excess of several minutes. This is longer than the timescale for generating DNP (∼seconds [53]). For this reason, we neglect nuclear dipolar interactions and diffusion in this work.

III. NUCLEAR SPIN-FLIP RATES AND KINETIC EQUATION

Before we describe our approach in detail, we first give an overview of the general strategy and main ingredients. Our framework is summarized in Fig. 2. The overall strategy is similar to that introduced in Refs. [72, 73]. However, significant modifications are needed to allow for higher nuclear spin. Also, here we present a non-perturbative approach, whereas Refs. [72, 73] relied on perturbation theory. Therefore, the theoretical model presented in this section has overlap with, but supersedes, that of Refs. [72, 73]. Readers who are only interested in the results and not the approach could skip ahead to Sec. IV.

We are dealing with a system that is both open and driven. An efficient way to treat non-unitary evolution is to use dynamical maps [72, 73, 109–111]. In this approach, the non-unitary evolution of a system from an initial state ρ to a final state ρ' is implemented by applying a set of operators and summing the results:

$$\rho' = \sum_k E_k \rho E_k^\dagger. \tag{7}$$

The operators E_k are known as Kraus operators, and they constitute a generalization of the usual unitary operators that evolve closed quantum systems to the case of non-unitary evolution in open systems. The condition $\sum_k E_k^\dagger E_k = \mathbb{1}$ ensures that the trace of the density matrix is always unity. The advantage of Kraus operators is that they allow one to incorporate effects due to the transient occupation of excited states using operators that live purely in the ground space of the system. In the present problem, we use these operators to describe the effect of each optical pulse on the electron spin state. The entire process of optical excitation, subsequent decay, and rotation is captured by an appropriate set of Kraus operators (given in Appendix A) without having to explicitly include excited states or a photonic bath into the formalism. The dynamical map description works well so long as the population returns regularly to the electron spin ground states, as is the case for the periodic driving used in the mode-locking experiments. These Kraus operators can then be used to obtain the electron spin steady state in the absence of nuclei, as shown in Appendix B.

Of course, we are interested in the case where the electron spin is coupled to a nuclear spin bath through HF interactions while it is being driven. Under the condition that the electron is being pumped fast enough (which indeed is the case for the mode-locking experiments [52–58]), the electron reaches its steady state on a much faster timescale compared to the electron-nuclear interaction dynamics and the electron spin decoherence time. This allows us to use a Markovian approximation in which we first solve for the driven electron steady state and then incorporate the effects due to the electron-nuclear couplings on top of this.

To bring the nuclei into the framework, we first solve for the joint evolution of one nuclear spin coupled to the driven electron spin. Although the HF interaction generates unitary dynamics, this is disrupted periodically by the pulses, and this in turn leads to an effective non-unitary dynamical map for the nuclear spin that depends on the electron steady state under the Markovian approximation. We extract nuclear spin-flip rates from this effective nuclear spin evolution operator; these rates provide information about the movement of population between the different nuclear spin levels.

We calculate the steady state of the entire nuclear spin bath using a rate equation that depends on the spin-flip rates obtained from the single-nucleus solution. A critical step is that we build in self-consistent system-environment feedback by modifying the flip rates. To understand this, we first need to describe the Overhauser effect [112], which is the main feedback mechanism be-

tween the electron and nuclei. A polarized nuclear spin bath acts as an effective magnetic field and therefore shifts the Zeeman frequency of the electron. However, the interaction between the electron and the nuclear spin bath is reciprocal; not only will the state of the electron change under the Overhauser field, but the nuclear spins will also be affected by the Knight field [113], i.e., the effective magnetic field due to polarization of the electron. The Knight field is given by the electron steady state spin vector, and so it enters into the nuclear spin flip rates, as explained above. The electron steady state (and hence the Knight field) in turn depends on the total magnetic field, which includes the Overhauser field due to nuclear polarization. These interdependencies constitute a complete feedback loop that must be treated self-consistently. We do this by making the nuclear spin-flip rates depend on the net nuclear polarization of the bath. The steady-state of the rate equation then gives the polarization distribution of the nuclear spin bath with feedback included. Finally, we use this nuclear polarization distribution to perform the Overhauser shift on the Zeeman frequency of the electron and update the nuclear-bath-averaged electron spin steady-state self-consistently.

The framework we have just outlined can be thought of as a self-consistent dynamical mean-field approach. In the remainder of this section, we use this approach to compute the dynamical map for a single nuclear spin as well as the nuclear spin flip rates. We then construct the kinetic equations that govern the dynamics of the full nuclear spin bath. Our method is quite general and can be applied to baths of any nuclear spin. Here, we focus on the cases $I = 1/2$, 1, and $3/2$.

A. Effective dynamical map for one nuclear spin

Given the electron spin steady state (Eq. (B5)), we can proceed to construct an effective dynamical map for a single nuclear spin. We do this by first constructing the evolution operator in the spin vector (SV) representation that describes the joint evolution of the electron and nuclear spins over one driving period. We then apply the Markovian approximation and reset the electron spin to its steady state at the end of the period. Tracing out the electron then leaves an effective dynamical map for the nuclear spin.

To start, we must choose a basis of Hermitian matrices $\hat{\lambda}_k$ of dimension $2I+1$, where $k = 1, \ldots, (2I+1)^2$, in order to define the nuclear SV. Unlike in the spin $I = 1/2$ case considered in Refs. [72, 73], for $I > 1/2$ we have much more freedom in how to choose this basis, and the choice we make can have a substantial impact on the complexity of the analysis that follows. We choose the first $2I + 1$ of these matrices to be diagonal, each with a single nonzero component equal to one. The remaining $2I(2I + 1)$ matrices each have two nonzero components, and these matrices are purely real or purely imaginary. For example, in the case of $I = 3/2$, we have 16 basis matrices:

$$
\begin{aligned}
&\hat{\lambda}_{k,ab} = \delta_{ak}\delta_{bk}, \quad k = 1 \ldots 4, \\
&\hat{\lambda}_{5,ab} = \tfrac{1}{\sqrt{2}}(\delta_{a1}\delta_{b2} + \delta_{a2}\delta_{b1}), \quad \hat{\lambda}_{6,ab} = \tfrac{-i}{\sqrt{2}}(\delta_{a1}\delta_{b2} - \delta_{a2}\delta_{b1}), \quad \hat{\lambda}_{7,ab} = \tfrac{1}{\sqrt{2}}(\delta_{a1}\delta_{b3} + \delta_{a3}\delta_{b1}), \\
&\hat{\lambda}_{8,ab} = \tfrac{-i}{\sqrt{2}}(\delta_{a1}\delta_{b3} - \delta_{a3}\delta_{b1}), \quad \hat{\lambda}_{9,ab} = \tfrac{1}{\sqrt{2}}(\delta_{a1}\delta_{b4} + \delta_{a4}\delta_{b1}), \quad \hat{\lambda}_{10,ab} = \tfrac{-i}{\sqrt{2}}(\delta_{a1}\delta_{b4} - \delta_{a4}\delta_{b1}), \\
&\hat{\lambda}_{11,ab} = \tfrac{1}{\sqrt{2}}(\delta_{a2}\delta_{b3} + \delta_{a3}\delta_{b2}), \quad \hat{\lambda}_{12,ab} = \tfrac{-i}{\sqrt{2}}(\delta_{a2}\delta_{b3} - \delta_{a3}\delta_{b2}), \quad \hat{\lambda}_{13,ab} = \tfrac{1}{\sqrt{2}}(\delta_{a2}\delta_{b4} + \delta_{a4}\delta_{b2}), \\
&\hat{\lambda}_{14,ab} = \tfrac{-i}{\sqrt{2}}(\delta_{a2}\delta_{b4} - \delta_{a4}\delta_{b2}), \quad \hat{\lambda}_{15,ab} = \tfrac{1}{\sqrt{2}}(\delta_{a3}\delta_{b4} + \delta_{a4}\delta_{b3}), \quad \hat{\lambda}_{16,ab} = \tfrac{-i}{\sqrt{2}}(\delta_{a3}\delta_{b4} - \delta_{a4}\delta_{b3}).
\end{aligned} \tag{8}
$$

These matrices are normalized such that $\mathrm{Tr}[\hat{\lambda}_j\hat{\lambda}_k] = \delta_{jk}$. Denoting the nuclear spin density matrix as ρ_n, the components of the nuclear SV $\mathcal{S}_n$ are then given by

$$\mathcal{S}_{n,k} = \mathrm{Tr}[\rho_n\lambda_k]. \tag{9}$$

Note that the populations, $\rho_{n,ii}$, are the first four components of $\mathcal{S}_n$. We will see that this feature simplifies the process of computing flip rates.

Let us denote the density matrix that describes the total electron-nuclear spin state at the beginning of a driving period by ϱ. We expand this in terms of an operator basis formed from tensor products of the nuclear spin operators $\hat{\lambda}_k$ with the electron spin Pauli matrices $\hat{\sigma}_j$:

$$\hat{G}_{(2I+1)^2 j+k} = \hat{\sigma}_j \otimes \hat{\lambda}_k, \tag{10}$$

with $j = 0, .., 3$, $k = 1, ..., (2I + 1)^2$, and where we define $\hat{\sigma}_0 = \mathbb{1}_{2\times2}$. We use this set of $4(2I + 1)^2$ operators as a basis for the SV of the joint system: $\mathcal{S}_\ell = \mathrm{Tr}(\varrho\hat{G}_\ell)$. This SV evolves over one driving period according to $\mathcal{S}' = \mathcal{Y}\mathcal{S}$, where the SV evolution operator $\mathcal{Y}$ is given by

$$\mathcal{Y}_{\ell\ell'} = \frac{1}{2}\mathrm{Tr}\left[\hat{G}_\ell\mathcal{U}\hat{G}_{\ell'}\mathcal{U}^\dagger\right], \tag{11}$$

where $\mathcal{U} = \exp\{-i(\omega_e\hat{S}_z + \omega_n\hat{I}_z + H_{HF}^{N=1} + H_Q^{N=1})T_R\}$ describes the joint evolution of the electron spin and single

nuclear spin under precession and the HF and quadrupolar interactions. At this point, we invoke the Markovian approximation: Because the electron reaches its steady state, $\mathcal{S}_e^{ss}$, quickly compared to the timescales for nuclear spin and HF dynamics, we reset the electron SV to its steady state value at the beginning/end of each period: $\mathcal{S} = \mathcal{S}_e^{ss} \otimes \mathcal{S}_n$. We then obtain an effective nuclear spin dynamical map, $\mathcal{Y}_n$, by acting with the full evolution operator, $\mathcal{Y}$, on the tensor product $\mathcal{S}_e^{ss} \otimes \mathcal{S}_n$ and reading off the coefficients of the components of the nuclear SV, $\mathcal{S}_n$, from the resulting $\mathcal{S}'$:

$$\mathcal{Y}_{n,jk} = \frac{d}{d\mathcal{S}_{n,k}} \left[\mathcal{Y}(\mathcal{S}_e^{ss} \otimes \mathcal{S}_n)\right]_j . \tag{12}$$

Here, $j, k = 1, ..., (2I+1)^2$, that is, we only retain the components of $\mathcal{S}'$ that correspond to the basis operators $\hat{G}_k = \mathbb{1}_{2\times 2} \otimes \hat{\lambda}_k$, i.e., the components that correspond to purely nuclear spin degrees of freedom. Note that although the joint evolution operator $\mathcal{Y}$ describes unitary evolution, the nuclear spin dynamical map, $\mathcal{Y}_n$, implements non-unitary evolution. This non-unitarity is a consequence of the Markovian approximation, which is itself due to the non-unitary driving of the electron spin.

B. Single-nucleus flip rates

We can use the nuclear spin dynamical map, $\mathcal{Y}_n$, that we found in the previous subsection to find the flip rates for a single nuclear spin interacting with the electron spin. These flip rates govern the movement of population from one nuclear spin state to another. Such processes are described by the following kinetic equation:

$$\frac{dp_m}{dt} = \sum_{n\neq m} \mathrm{w}_n^m p_n - \sum_{n\neq m} \mathrm{w}_m^n p_m, \tag{13}$$

where p_m is the population of level m, and w_n^m is the rate to flip from state n to m, which in general differs from the rate to flip from m to n, w_m^n. Which transitions are allowed depends on the type of interactions present in the Hamiltonian. For instance, the HF flip-flop terms only cause $\Delta m_I = \pm 1$ transitions, while the quadrupolar interaction also drives $\Delta m_I = \pm 2$ transitions. We can combine the rate equations (13) into a matrix equation. We exemplify this in the $I = 3/2$ case, where we denote the four states $|+3/2\rangle$, $|+1/2\rangle$, $|-1/2\rangle$, $|-3/2\rangle$, by the shorthand $\{++, +, -, --\}$. The matrix equation is then $\dot{\mathcal{P}} = \mathcal{M}\mathcal{P}$, where $\mathcal{P} = (p_{++}, p_+, p_-, p_{--})$, and

$$\mathcal{M} = \begin{bmatrix} -(\mathrm{w}_{++}^{+} + \mathrm{w}_{++}^{-} + \mathrm{w}_{++}^{--}) & \mathrm{w}_{+}^{++} & \mathrm{w}_{-}^{++} & \mathrm{w}_{--}^{++} \\ \mathrm{w}_{++}^{+} & -(\mathrm{w}_{+}^{++} + \mathrm{w}_{+}^{-} + \mathrm{w}_{+}^{--}) & \mathrm{w}_{-}^{+} & \mathrm{w}_{--}^{+} \\ \mathrm{w}_{++}^{-} & \mathrm{w}_{+}^{-} & -(\mathrm{w}_{-}^{++} + \mathrm{w}_{-}^{+} + \mathrm{w}_{-}^{--}) & \mathrm{w}_{--}^{-} \\ \mathrm{w}_{++}^{--} & \mathrm{w}_{+}^{--} & \mathrm{w}_{-}^{--} & -(\mathrm{w}_{--}^{+} + \mathrm{w}_{--}^{-} + \mathrm{w}_{--}^{++}) \end{bmatrix}. \tag{14}$$

It is clear that this equation satisfies the condition that the sum of the components of the probability vector $\mathcal{P}$ should be unity at all times. This is guaranteed by the property that the sum of the rows of $\mathcal{M}$ vanishes.

To determine the flip rates, we need to connect the generic kinetic equation, Eq. (13), to the nuclear spin evolution operator, Eq. (12), derived earlier. This can be done by starting from the evolution over one driving period:

$$\mathcal{S}_n(t + T_R) = \mathcal{Y}_n \mathcal{S}_n(t). \tag{15}$$

The fact that the nuclear spin evolution is much slower than the driving period T_R allows us to coarse-grain this equation to arrive at a continuous evolution equation:

$$\frac{d}{dt}\mathcal{S}_n = \frac{1}{T_R}(\mathcal{Y}_n - \mathbb{1})\mathcal{S}_n. \tag{16}$$

Because we have defined $\mathcal{S}_n$ such that its first four components are just the populations of the nuclear spin states, we can identify this equation with $\dot{\mathcal{P}} = \mathcal{M}\mathcal{P}$ and therefore read off the flip-rate matrix components from the nuclear spin evolution matrix:

$$\mathcal{M}_{ij} = \frac{1}{T_R}(\mathcal{Y}_n - \mathbb{1})_{ij}, \quad i, j = 1...2I+1. \tag{17}$$

This allows us to read off the flip rates from the nuclear spin dynamical map. It is worth noting that $\mathcal{Y}_n$ contains not only terms that mix the populations of the different nuclear spin levels but also terms that mix populations and nuclear spin coherences. Here, we are neglecting the influence of the latter on the late-time populations. In numerical simulations, we find that these terms have a negligible effect on the flip rates. Moreover, they will be further suppressed by nuclear spin dephasing [7, 32], which happens quickly compared to nuclear spin flips. This simplification allows us to obtain non-perturbative expressions for the flip rates.

In the case of $I = 1/2$ nuclei, the flip rates can be obtained analytically following the above procedure:

$$\mathrm{w}_{\pm} = \frac{A^2(1 \pm S_{e,z}^{ss}) \sin^2(T_R\sqrt{(\omega_e - \omega_n)^2 + A^2}/2)}{2T_R[(\omega_e - \omega_n)^2 + A^2]}, \tag{18}$$

where we use the shorthand notation $\mathrm{w}_+ \equiv \mathrm{w}_{-1/2}^{+1/2}$ and $\mathrm{w}_- \equiv \mathrm{w}_{+1/2}^{-1/2}$. Note that unlike in Refs. [72, 73], here we did not have to resort to perturbation theory in the HF interaction to obtain an analytical expression for the flip rates. The flip rates for $I = 1$ and $I = 3/2$ can also

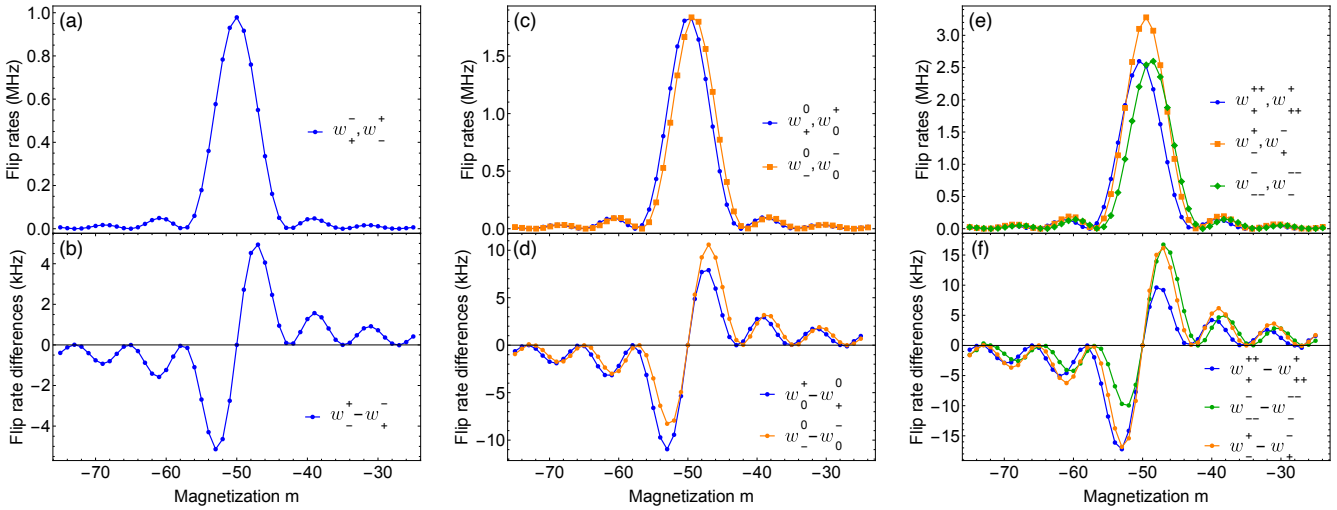

FIG. 3. Single-nucleus spin-flip rates for (a,b) $I = 1/2$, (c,d) $I = 1$, (e,f) $I = 3/2$ as a function of the magnetization m of the nuclear spin bath. Flip rates are shown in (a), (c), (e), while flip rate differences are shown in (b), (d), (f). The parameter values are $T_R = 13.2$ ns, $NA = 10$ GHz, $N = 1000$, $\omega_{e0} = 0.5$ GHz, $\omega_n = -0.5$ MHz, $\gamma_e = 0.5$ GHz, $q_0 = 0.3$, $\phi = -\pi/2$. For (c-f), we set the quadrupolar parameters to $\nu_Q = 2.8$ MHz and $\theta = 0$. Only the nonzero flip rates are shown.

be obtained analytically in the case of zero quadrupolar coupling, $\nu_Q = 0$. In this case, there are four nonzero flip rates for $I = 1$:

$$
\begin{aligned}
\mathrm{w}_{-1}^{0} &= \frac{A^2(1+S_{e,z}^{ss})\sin^2(T_R\Omega_{-}^{(1)}/2)}{T_R(\Omega_{-}^{(1)})^2},\\
\mathrm{w}_{0}^{-1} &= \frac{A^2(1-S_{e,z}^{ss})\sin^2(T_R\Omega_{-}^{(1)}/2)}{T_R(\Omega_{-}^{(1)})^2},\\
\mathrm{w}_{0}^{+1} &= \frac{A^2(1+S_{e,z}^{ss})\sin^2(T_R\Omega_{+}^{(1)}/2)}{T_R(\Omega_{+}^{(1)})^2},\\
\mathrm{w}_{+1}^{0} &= \frac{A^2(1-S_{e,z}^{ss})\sin^2(T_R\Omega_{+}^{(1)}/2)}{T_R(\Omega_{+}^{(1)})^2},
\end{aligned}
\tag{19}
$$

with

$$
\Omega_{\pm}^{(1)} = \sqrt{(\omega_e-\omega_n)^2 \pm A(\omega_e-\omega_n) + 9A^2/4}, \tag{20}
$$

while there are six nonzero flip rates for $I = 3/2$:

$$
\begin{aligned}
\mathrm{w}_{+}^{++} &= \frac{3A^2(1+S_{e,z}^{ss})\sin^2(T_R\Omega_{+1}^{(3/2)}/2)}{2T_R(\Omega_{+1}^{(3/2)})^2},\\
\mathrm{w}_{++}^{+} &= \frac{3A^2(1-S_{e,z}^{ss})\sin^2(T_R\Omega_{+1}^{(3/2)}/2)}{2T_R(\Omega_{+1}^{(3/2)})^2},\\
\mathrm{w}_{-}^{+} &= \frac{A^2(1+S_{e,z}^{ss})\sin^2(T_R\Omega_{0}^{(3/2)}/2)}{T_R(\Omega_{0}^{(3/2)})^2},\\
\mathrm{w}_{+}^{-} &= \frac{A^2(1-S_{e,z}^{ss})\sin^2(T_R\Omega_{0}^{(3/2)}/2)}{T_R(\Omega_{0}^{(3/2)})^2},\\
\mathrm{w}_{--}^{-} &= \frac{3A^2(1+S_{e,z}^{ss})\sin^2(T_R\Omega_{-1}^{(3/2)}/2)}{2T_R(\Omega_{-1}^{(3/2)})^2},\\
\mathrm{w}_{-}^{--} &= \frac{3A^2(1-S_{e,z}^{ss})\sin^2(T_R\Omega_{-1}^{(3/2)}/2)}{2T_R(\Omega_{-1}^{(3/2)})^2},
\end{aligned}
\tag{21}
$$

with

$$
\Omega_{\eta}^{(3/2)} = \sqrt{(\omega_e-\omega_n)^2 + 2\eta A(\omega_e-\omega_n) + 4A^2}. \tag{22}
$$

In the absence of quadrupolar interactions, only $\Delta m_I = \pm 1$ transitions (i.e., transitions between adjacent spin levels) are allowed, as follows directly from the form of the HF flip-flop interaction. When the quadrupolar coupling is nonzero, we can no longer obtain an analytical expression for the flip rates, but these are still easily obtained numerically by computing $\mathcal{Y}_n$ for specific parameter values.

C. Multi-nuclear flip rates

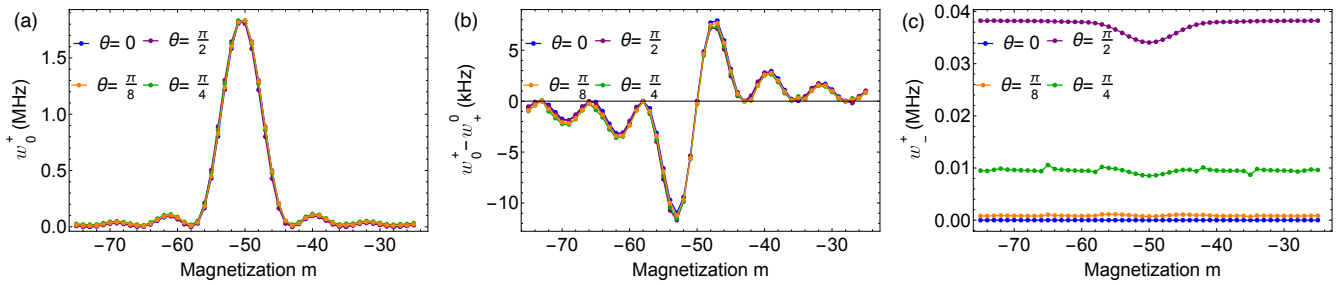

FIG. 4. Single-nucleus spin-flip rates as a function of nuclear spin bath magnetization m for $I = 1$ and for different values of the quadrupolar angle θ. (a) Flip rate for the $\Delta m_I = 1$ transition $|0\rangle \to |+1\rangle$. (b) Flip rate difference for the $|0\rangle \leftrightarrow |+1\rangle$ transitions. (c) Flip rate for the $\Delta m_I = 2$ transition $|-1\rangle \to |+1\rangle$. The parameter values are $T_R = 13.2$ ns, $NA = 10$ GHz, $N = 1000$, $\omega_{e0} = 0.5$ GHz, $\omega_n = -0.5$ MHz, $\gamma_e = 0.5$ GHz, $q_0 = 0.3$, $\phi = -\pi/2$, $\nu_Q = 2.8$ MHz.

We can convert the single-nucleus flip rates obtained above into multi-nuclear flip rates by making them dependent on the magnetization of the entire nuclear spin bath. This dependence comes from the Overhauser effect in which nuclear spin polarization acts as an effective magnetic field seen by the electron spin. We incorporate this effect by adding a magnetization-dependent shift to the precession frequency of the electron:

$$w_i^j(m) = \mathrm{w}_i^j(\omega_e \to \omega_{e0} + mA), \tag{23}$$

where ω_{e0} denotes the contribution to the precession frequency due purely to the external magnetic field, and where we use $w_i^j(m)$ to denote the rate to flip from state i to state j in the presence of nuclear spin magnetization m. For nuclei of spin I, we can express this magnetization in terms of occupation numbers, N_ℓ, for each of the nuclear spin states:

$$m = \sum_{\ell=-I}^{I} \ell\, N_\ell. \tag{24}$$

Fig. 3 shows the dependence of the flip rates on the net magnetization m for $I = 1/2$, 1, and $3/2$. In this figure, results for zero quadrupolar angle, $\theta = 0$, are shown in the $I > 1/2$ cases. Even though the quadrupolar coupling is nonzero, $\nu_Q > 0$, only $\Delta m_I = \pm 1$ transitions are permitted in this case because when $\theta = 0$, the only effect of the quadrupolar interaction is to modify the energy splittings between nuclear spin levels, and so the selection rules are still determined solely by the HF interaction. We discuss the effect of nonzero θ below.

The salient features evident in Fig. 3 can be understood from the non-perturbative expressions for the flip rates given above. First of all, the flip rates are strongly peaked at magnetization $m \approx -\omega_{e0}/A$. In the spin 1/2 case, the precise location of the peak is the value of m at which the argument of the sine in Eq. (18) vanishes since the flip rates are essentially given by squared sinc functions. For low to moderate external magnetic field strengths and large N, the terms involving ω_n and A^2 can be neglected, leaving $m \approx -\omega_{e0}/A$. Similar statements hold for $I = 1$ and $I = 3/2$ in the absence of quadrupolar effects, as is clear from Eqs. (19) and (21). The fact that the flip rates are maximal at $m \approx -\omega_{e0}/A$ can be understood from energy conservation: At these values, the effective Zeeman energy of the electron is almost zero, and thus so is the energy mismatch between the electron and nucleus. This in turn reduces the energy penalty for flip-flops, accelerating the transfer of polarization. Conversely, the overall decay of the flip rates away from $m \approx \omega_{e0}/A$ is due to the HF interaction becoming inefficient at overcoming the large energy mismatch between the electronic and nuclear spin splittings.

It is also evident in Fig. 3 that the flip rates vanish periodically as a function of m. The periodicity is also controlled by the arguments of the sine functions in the flip rates. These zeros correspond to values of ω_e for which complete flip-flops between the electronic and nuclear spins occur—polarization is transferred back and forth between the electron and nucleus an integer number of times within a single drive period T_R. Because there is no net polarization transfer, the flip rate vanishes. For $I > 1/2$, the locations of these zeros depend on which pair of adjacent spin levels we consider, although this dependence fades away in the large N limit, where $A \to 0$. In the next section, we show that these flip-rate zeros play a central role in the phenomenon of mode-locking.

Each pair of flip rates describing transitions between the same two spin levels are almost equal [see panels (b), (d), (f) of Fig. 3]. As can be seen from Eqs. (18)-(21), the differences of these flip rates are proportional to $S^{ss}_{e,z}(m)$, and this component of the electron steady state is suppressed near $m \approx -\omega_{e0}/A$ because it is proportional to ω_e (see Eq. (B5)). This is a reflection of the fact that when $\omega_e = 0$, the electron steady state becomes polarized along the optical pulse axis (the x direction), where it is no longer affected by the pulses and is thus stabilized. In the figure, we see that this combination of accelerated flip-flops and the suppression of $S^{ss}_{e,z}(m)$ near $m \approx -\omega_{e0}/A$ results in flip rate differences that are more than two orders of magnitude smaller than the flip rates themselves.

The effect of a nonzero quadrupolar angle θ on the flip rates is shown in Figs. 4 and 5 for $I = 1$ and $3/2$, re-

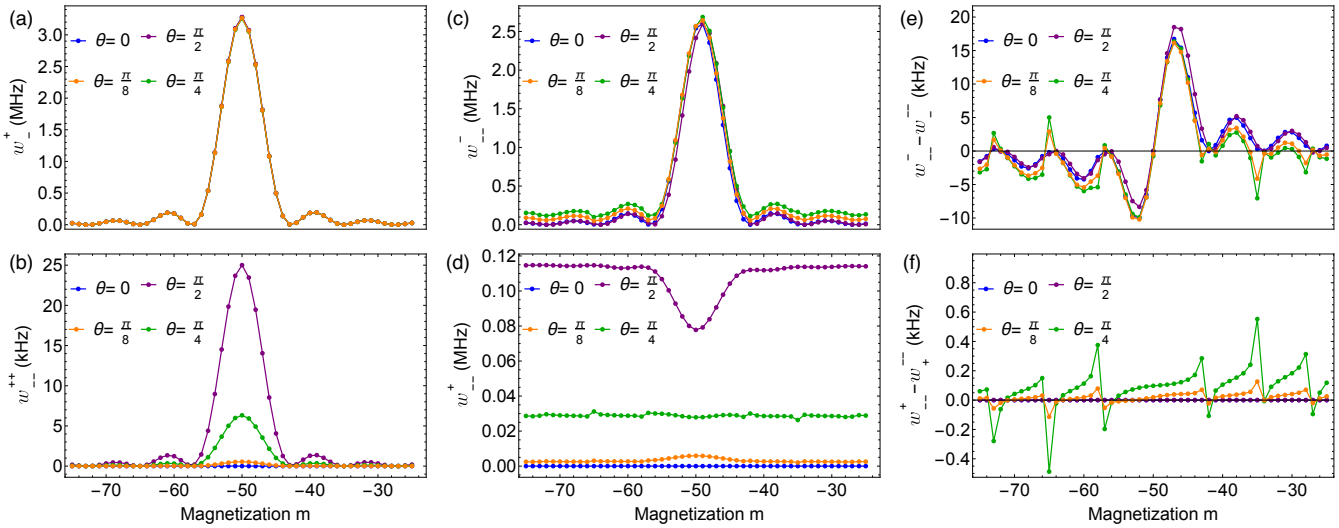

FIG. 5. Single-nucleus spin-flip rates as a function of nuclear spin bath magnetization m for $I = 3/2$ and for different values of the quadrupolar angle θ. (a) Flip rate for the $\Delta m_I = 1$ transition $|-1/2\rangle \to |+1/2\rangle$. (b) Flip rate for the $\Delta m_I = 3$ transition $|-3/2\rangle \to |+3/2\rangle$. (c) Flip rate for the $\Delta m_I = 1$ transition $|-3/2\rangle \to |-1/2\rangle$. (d) Flip rate for the $\Delta m_I = 2$ transition $|-3/2\rangle \to |+1/2\rangle$. (e) Flip rate difference for the $|-3/2\rangle \leftrightarrow |-1/2\rangle$ transitions. (f) Flip rate difference for the $|-3/2\rangle \leftrightarrow |+1/2\rangle$ transitions. The parameter values are $T_R = 13.2$ ns, $NA = 10$ GHz, $N = 1000$, $\omega_{e0} = 0.5$ GHz, $\omega_n = -0.5$ MHz, $\gamma_e = 0.5$ GHz, $q_0 = 0.3$, $\phi = -\pi/2$, $\nu_Q = 2.8$ MHz.

spectively. In the case $I = 1$, it is evident that θ has a negligible effect on the $\Delta m_I = \pm 1$ flip rates. On the other hand, sufficiently large values of the angle, $\theta \gtrsim \pi/4$, give rise to $\Delta m_I = \pm 2$ transitions that are not otherwise present. Although the rates for these transitions are two orders of magnitude smaller than those of the $\Delta m_I = \pm 1$ transitions, they are still large enough to affect the polarization distribution of the nuclear spin bath, as we show in Sec. IV. Similar but somewhat more prominent effects are evident for $I = 3/2$ in Fig. 5. Here, larger values of θ produce small but noticeable changes in $\Delta m_I = \pm 1$ flip rates, significant $\Delta m_I = \pm 2$ transition rates, and even $\Delta m_I = \pm 3$ transitions. A striking feature evident in both Figs. 4 and 5 is that the flip rates for $\Delta m_I = \pm 2$ transitions do not decay as m moves away from $m = -\omega_{e0}/A$. This is consistent with the fact that spin flips caused by the quadrupolar interaction do not require the electron and nuclear spin Zeeman energies to be equal. Unlike HF spin flips, quadrupolar spin flips depend weakly on the bath magnetization. On the other hand, the $\Delta m_I = \pm 3$ flip rates are sensitive to m (see Fig. 5(b)), because these arise from a higher-order process that combines HF and quadrupolar spin flips.

D. Kinetic equations for multi-nuclear spin polarization distributions

In this subsection, we use the flip rates obtained in the previous subsection to construct kinetic rate equations that govern the evolution of the polarization distribution of the entire nuclear spin bath. We do this for each of the three values of nuclear total spin I considered in this work. Although the kinetic equation for $I = 1/2$ has been discussed in detail elsewhere [72, 73], here we present an analytical solution to this equation that was not previously known. The kinetic equations for $I = 1$ and $3/2$ will be solved numerically in the next section to obtain nuclear spin polarization distributions in these cases. Detailed comparisons of the polarization distributions that result in all three cases for various parameter values are given below in Sec. IV. In that section, these distributions are then used to compute the effect on the electron spin evolution with and without quadrupolar interactions.

1. *Kinetic equation for spin $I = 1/2$ nuclei*

The polarization of a spin 1/2 nuclear bath in a definite configuration with occupation numbers N_+ and N_- (the number of spins in the $|+1/2\rangle$ and $|-1/2\rangle$ states, respectively) is given by $m = (N_+ - N_-)/2$. The total number of spins is $N = N_+ + N_-$. Knowledge of the polarization m is sufficient to determine the two occupation numbers, N_+ and N_-. This in turn means that the probability of each bath configuration is equal to the polarization probability distribution $P(m)$. We may write down a kinetic equation governing the dynamics of this distribution [72, 73]:

$$\frac{d}{dt}P(m) = -\sum_{\pm}\left[w_{\pm}(m)\frac{N \mp 2m}{2}\right]P(m) + \sum_{\pm} w_{\mp}(m \pm 1)\left[\frac{N \pm 2m}{2} + 1\right]P(m \pm 1). \tag{25}$$

A close look at this kinetic equation reveals that the right-hand side is comprised of two terms that are related to each other by shifting $m \to m+1$:

$$\frac{d}{dt}P(m) = F(m+1) - F(m), \tag{26}$$

where $F(m) = w_-(m)(m+N/2)P(m) - w_+(m-1)(-m+1+N/2)P(m-1)$. Therefore, in the steady state where $dP(m)/dt = 0$, we find $F(m) = F(m+1) =$ constant. Since we must have $P(N+1) = 0$, it follows that this constant is zero. The equation $F(m) = 0$ then yields a two-term recursion relation [72, 73]:

$$P(m) = \frac{N-2m+2}{N+2m}\,\frac{w_+(m-1)}{w_-(m)}P(m-1). \tag{27}$$

This relation can easily be solved iteratively starting from an arbitrary value for $P(-N)$ and then imposing the normalization condition $\sum_m P(m) = 1$. This approach was used to produce numerical results for the polarization distribution in Refs. [72, 73]. Notice that this procedure yields the unique steady state of the kinetic equation, Eq. (25). Because of this uniqueness, the steady state must be stable. This is evident from the kinetic equation, where a positive fluctuation that takes $P(m)$ away from its steady-state value results in $dP(m)/dt < 0$, which indicates that the steady state will be subsequently restored. An analogous statement holds for a negative fluctuation as well. The kinetic equations for $I > 1/2$ described below also possess this property.

Here, we obtain an analytical solution for $P(m)$ by exploiting the explicit, non-perturbative expressions we obtained for the flip rates in Eq. (18). First of all, an expression for $P(m)$ follows immediately from Eq. (27):

$$\begin{aligned} P(m) &= \mathcal{N}^{-1}\prod_{k=1-N/2}^{m}\frac{N-2k+2}{N+2k}\,\frac{w_+(k-1)}{w_-(k)} \\ &= \frac{\mathcal{N}^{-1}N!}{(N/2+m)!(N/2-m)!}\prod_{k=1-N/2}^{m}\frac{w_+(k-1)}{w_-(k)}, \end{aligned} \tag{28}$$

where $\mathcal{N}$ is a normalization factor. Next, we use the fact that the two flip rates only differ by the sign in front of $S^{ss}_{e,z}(m)$, which leads to a cascade of cancellations between the numerator and denominator in the product. We are left with

$$\begin{aligned} P(m) = &\frac{\mathcal{N}^{-1}}{(N/2+m)!(N/2-m)!}\prod_{k=1-N/2}^{m}\frac{1+S^{ss}_{e,z}(k-1)}{1-S^{ss}_{e,z}(k)} \\ &\times\frac{(\omega_{e0}-\omega_n+Am)^2+A^2}{\sin^2(T_R\sqrt{(\omega_{e0}-\omega_n+Am)^2+A^2}/2)}, \end{aligned} \tag{29}$$

where we have absorbed additional constants into $\mathcal{N}$. The first, combinatoric factor in $P(m)$ corresponds to a Gaussian-like envelope that quickly approaches a Gaussian as N increases: $[(N/2)!]^2/[(N/2+m)!(N/2-m)!] \to e^{-2m^2/N}$ as $N \to \infty$. The second factor in Eq. (29) produces sharp spikes at values of m that correspond to the zeros of the flip rates. These values of m satisfy

$$\sqrt{(\omega_{e0}-\omega_n+Am)^2+A^2} \approx \frac{2\pi p}{T_R}, \tag{30}$$

where p is an integer. The concentration of probability near these special values of m produces mode-locking: Nuclear polarization shifts the electron Zeeman frequency to values where HF flip-flops stop transferring polarization between the electronic and nuclear spins. This happens because an integer number of flip-flops occur during each drive period. Using that $\omega_n \ll \omega_{e0}$ and assuming N is sufficiently large that $A \ll \omega_{e0}$, these values of m correspond to the electron precession becoming commensurate with the pulse train: $\omega_e = \omega_{e0} + Am \approx 2\pi p/T_R$, which is the primary signature of mode-locking seen in experiments [52–58].

The middle factor (the product) in Eq. (29) is primarily responsible for the average magnetization of the nuclear spin bath, $\langle m\rangle = \sum_m mP(m)$. This factor is also where additional pulse parameters such as the rotation angle ϕ and the residual ground state population q_0 influence the polarization distribution. If ϕ is equal to 0 or π or if q_0 is zero, then $S^{ss}_{e,z}(k) = 0$ for all k, in which case the final factor in Eq. (29) reduces to 1. In this case, the combinatoric factor, which is centered about $m = 0$, ensures that the average magnetization will be small, $\langle m\rangle \approx 0$. On the other hand, if $\phi \neq 0$ and the external magnetic field is sufficiently large, then $\langle m\rangle$ can be significant, and its sign depends on the sign of ϕ and on the orientation of the external field. If $\phi > 0$, then $S^{ss}_{e,z}(m)$ is more often positive than negative for $m < -\omega_{e0}/A$, which in turn means that $\frac{1+S^{ss}_{e,z}(m-1)}{1-S^{ss}_{e,z}(m)}$ is biased toward values larger than 1, and so the product grows as m increases. Once m passes $-\omega_{e0}/A$, $S^{ss}_{e,z}(m)$ now tends to more negative values, and the product shrinks as m increases. Thus, we see that for $\phi > 0$, the product in Eq. (29) is peaked at $m \approx -\omega_{e0}/A$, and so the average magnetization will lie between 0 and $-\omega_{e0}/A$. On the other hand, if $\phi < 0$, then the same reasoning leads to the conclusion that the product in Eq. (29) has a dip at $m \approx -\omega_{e0}/A$, and thus the net magnetization is driven away from this point and will have a sign that coincides with that of ω_{e0}. These features are borne out in plots of Eq. (29), as shown below in Sec. IV.

2. *Kinetic equation for spin $I = 1$ nuclei*

Before we write down the kinetic equation for $I = 1$ nuclei, we first introduce the notation we use to distinguish different bath configurations. We denote the occupation numbers of the three spin states by N_{-1}, N_0, and N_1. The bath polarization for a given configuration is then $m = +1 \times N_1 + 0 \times N_0 - 1 \times N_{-1}$. We see immediately that there is an important difference compared to the

$I = 1/2$ case considered above: The polarization does not uniquely specify a configuration of the bath. For instance, in the case of two $I = 1$ spins with $m = 0$, we can have either $N_1 = 1 = N_{-1}$ and $N_0 = 0$ or $N_1 = 0 = N_{-1}$ and $N_0 = 2$. This is in contrast to the $I = 1/2$ case, where each value of m corresponds to a unique configuration. As the number of spins increases, the number and orders of such "degeneracies" grow quickly. Because the polarization does not uniquely specify a configuration, we must combine it with one of the occupation numbers to uniquely label different configurations. We choose to use N_0 and express the probability of a given configuration by $P(m, N_0)$. Unlike in the spin 1/2 case, this quantity is now distinct from the polarization probability distribution; the latter is obtained by summing over all possible values of N_0 that are consistent with the given value of m:

$$P(m) = \sum_{N_0} P(m, N_0). \tag{31}$$

We can write down a kinetic equation for $P(m, N_0)$:

$$\frac{d}{dt}P(m, N_0) = F(m, N_0) + G(m + 1, N_0 - 1) \\ -G(m, N_0) - F(m + 1, N_0 + 1), \tag{32}$$

where

$$F(m, N_0) = -w_0^{-1}P(m, N_0)N_0 \tag{33}$$
$$+w_{-1}^0(m - 1)P(m - 1, N_0 - 1)N_-(m - 1, N_0 - 1),$$
$$G(m, N_0) = w_1^0P(m, N_0)N_+(m, N_0)$$
$$-w_0^1(m - 1)P(m - 1, N_0 + 1)(N_0 + 1). \tag{34}$$

Here $N_\pm(m, N_0) \equiv (1/2)(N \pm m - N_0)$. In the kinetic equation above we have only considered the $\Delta m_I = \pm 1$ transitions. Including transitions that change the angular momentum by more than 1 (for instance due to quadrupolar interactions) leads to additional terms not shown above. Such terms are illustrated for the case of $I = 3/2$ nuclei in the next section. Returning to the spin 1 case, the steady state of the above kinetic equation,

$$F(m, N_0)-G(m, N_0) = F(m+1, N_0+1)-G(m+1, N_0-1), \tag{35}$$

does not yield a recursion relation as in the $I = 1/2$ case. We solve this equation (and its generalization for nonzero quadrupolar interactions) numerically in Sec. IV.

3. *Kinetic equation for spin $I = 3/2$ nuclei*

We again adopt the notation $\{++, +, -, --\}$ to label quantities associated with the four spin quantum numbers $m_I = \{+3/2, +1/2, -1/2, -3/2\}$ of a spin 3/2 nucleus. For a nuclear spin bath comprised of $N = N_{++} + N_+ + N_- + N_{--}$ spins, the magnetization of the system (Eq. (24)) is $m = (3N_{++} + N_+ - N_- - 3N_{--})/2$. In the $I = 3/2$ case, we need two more quantities in addition to m to uniquely label different multi-spin configurations. We choose these to be N_{++} and N_{--}. The remaining two occupation numbers are then determined by these three quantities for a fixed total number of spins:

$$N_+ = \frac{1}{2}(2m + N - 4N_{++} + 2N_{--}), \tag{36}$$

$$N_- = \frac{1}{2}(-2m + N + 2N_{++} - 4N_{--}). \tag{37}$$

The probabilities $P(m, N_{++}, N_{--})$ that the nuclear spin bath is in the various configurations labeled by m, N_{++}, and N_{--} obey the following set of kinetic equations:

$$\frac{d}{dt}P(m, N_{++}, N_{--}) = F(m, N_{++}, N_{--}) + G(m, N_{++}, N_{--}) + H(m, N_{++}, N_{--}) \\ +I(m, N_{++}, N_{--}) + J(m, N_{++}, N_{--}) \\ -F(m + 1, N_{++} + 1, N_{--}) - G(m + 1, N_{++}, N_{--} - 1) - H(m + 1, N_{++}, N_{--}) \\ -I(m - 2, N_{++} - 1, N_{--}) - J(m + 2, N_{++}, N_{--} - 1), \tag{38}$$

where

$$F(m,N_{++},N_{--}) = +w_{+}^{++}(m-1)P(m-1,N_{++}-1,N_{--})N_{+}(m-1,N_{++}-1,N_{--}) \\ -w_{++}^{+}(m)P(m,N_{++},N_{--})N_{++}, \tag{39}$$

$$G(m,N_{++},N_{--}) = +w_{--}^{-}(m-1)P(m-1,N_{++},N_{--}+1)(N_{--}+1) \\ -w_{-}^{--}(m)P(m,N_{++},N_{--})N_{-}(m,N_{++},N_{--}), \tag{40}$$

$$H(m,N_{++},N_{--}) = +w_{-}^{+}(m-1)P(m-1,N_{++},N_{--})N_{-}(m-1,N_{++},N_{--}) \\ -w_{+}^{-}(m)P(m,N_{++},N_{--})N_{+}(m,N_{++},N_{--}), \tag{41}$$

$$I(m,N_{++},N_{--}) = +w_{++}^{-}(m+2)P(m+2,N_{++}+1,N_{--})(N_{++}+1) \\ -w_{-}^{++}(m)P(m,N_{++},N_{--})N_{-}(m,N_{++},N_{--}), \tag{42}$$

$$J(m,N_{++},N_{--}) = +w_{--}^{+}(m-2)P(m-2,N_{++},N_{--}+1)(N_{--}+1) \\ -w_{+}^{--}(m)P(m,N_{++},N_{--})N_{+}(m,N_{++},N_{--}). \tag{43}$$

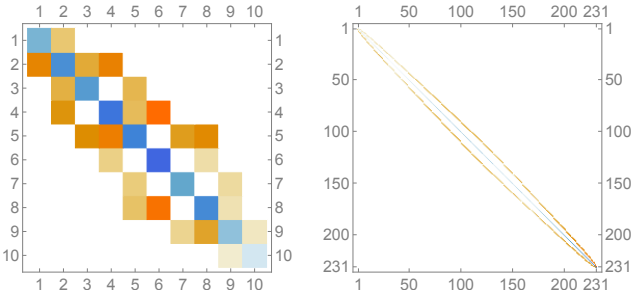

FIG. 6. Structure of the matrix $\mathcal{R}$ defining the linear system of equations governing the steady-state solution of the multi-nuclear kinetic equation for spin $I = 1$ for (left) $N = 3$ spins and (right) $N = 20$ spins in the absence of quadrupolar interactions.

Here, we have included $\Delta m_I = \pm 1$ and $\Delta m_I = \pm 2$ transitions. Although $\Delta m_I = \pm 3$ transitions cannot be directly driven by either the HF interaction or the quadrupolar interaction to first order in their respective coupling strengths, they can potentially arise from higher-order effects as we saw from the flip rates in Fig. 5. Now that we have the kinetic equations governing the nuclear polarization, the next step is to solve them.

IV. NUCLEAR POLARIZATION DISTRIBUTION AND FEEDBACK

A. Steady-state polarization distributions

For $I = 1$ and $I = 3/2$, we solve the respective kinetic equations numerically to obtain steady-state polarization distributions. This is done by first setting the time derivatives to zero: $\frac{d}{dt}P(m,N_{++},N_{--}) = 0$. The resulting algebraic equations are then collected together and written as a matrix $\mathcal{R}$ acting on a vector $\mathcal{V}$ of the probabilities $P(m,N_{++},N_{--})$ such that $\mathcal{R}\mathcal{V} = 0$. Thus, the steady-state polarization distribution is the unique null vector of $\mathcal{R}$. The matrix $\mathcal{R}$ depends on the Overhauser-shifted flip rates and occupation numbers for each configuration. The linear dimension of this matrix is equal to the number of distinct multi-spin configurations. For N spins of total spin I, the number of configurations is given by the simplicial polytopic numbers $\binom{N+2I}{2I}$. For $I = 1/2$, 1, and 3/2, this gives $N+1$, $(N+1)(N+2)/2$, and $(N+1)(N+2)(N+3)/6$, respectively. Therefore, in the case of $I = 1$, we must compute the null vector of a matrix that grows quadratically with the number of nuclei, while for $I = 3/2$, we must do the same for a matrix that grows like N^3. The matrix $\mathcal{R}$ is quite sparse in both cases (see Fig. 6), especially in the absence of quadrupolar interactions. This allows us to employ the Arnoldi method to compute the steady-state polarization distribution for hundreds of spins with $I = 3/2$ and thousands of spins with $I = 1$.

Fig. 7 compares results for the steady-state nuclear spin polarization for $N = 200$ for all three values of I. In the $I > 1/2$ cases, we set the quadrupolar angle to zero, $\theta = 0$; however, the nonzero quadrupolar interaction $\nu_Q > 0$ still modifies the energy splittings between the nuclear spin levels. In all three cases, the polarization distribution exhibits multiple narrow peaks at values of m that correspond to the mode-locking frequencies, i.e., these values of m are such that $\omega_{e0} + Am = 2\pi p/T_R$ where p is an integer (for an analytical derivation of the $I = 1/2$ case see Section III D 1). As discussed in Sec. III B, the flip rates approximately vanish at these values of m. (Note that the spacing of the peaks in Fig. 7 is five times smaller than the spacing of the flip-rate zeros in Figs. 3, 4, and 5 because this spacing is proportional to $1/A = N/\mathcal{A}$, and N is five times smaller in Fig. 7.) The steady-state probabilities $P(m,N_{++},N_{--})$ are largest at these magnetization values because they are multiplied by nearly vanishing flip rates in the kinetic equations; the probabilities must compensate for the smallness of the flip rates such that the product of the two is finite and comparable to terms of similar size in the kinetic equations. This trend can be seen explicitly from the an-

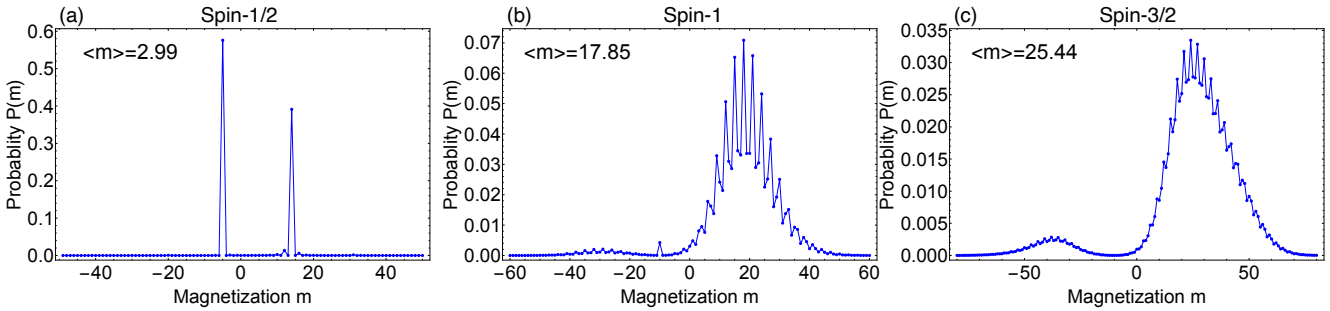

FIG. 7. Steady-state nuclear spin polarization distribution of a bath with $N = 200$ nuclear spins for (a) $I = 1/2$, (b) $I = 1$, and (c) $I = 3/2$. The parameter values are $T_R = 13.2$ ns, $NA = 10$ GHz, $\omega_{e0} = 0.5$ GHz, $\omega_n = -0.5$ MHz, $\gamma_e = 0.5$ GHz, $q_0 = 0.3$, $\phi = -\pi/2$, $\nu_Q = 2.8$ MHz. In the case of $I = 3/2$ and $I = 1$ the quadrupolar angle is $\theta = 0$.

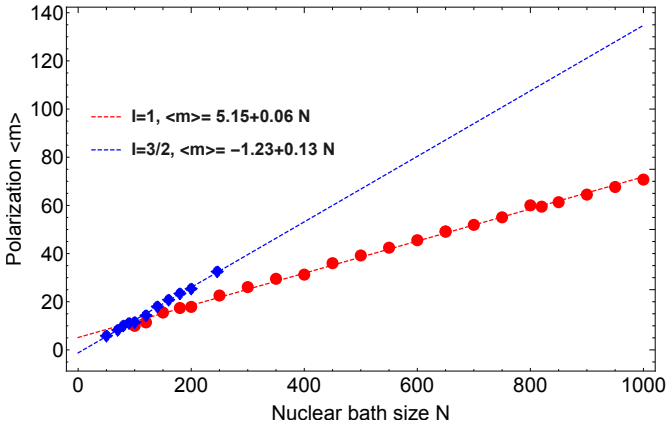

FIG. 8. Extrapolation of the average nuclear spin bath polarization $\langle m \rangle$ to larger bath sizes N for two values of total spin: $I = 1$ (red circles) and $I = 3/2$ (blue diamonds). The points are obtained by solving the respective kinetic equations, Eqs. (32) and (38). The lines are linear fits. The parameter values are $T_R = 13.2$ ns, $NA = 10$ GHz, $\omega_{e0} = 0.5$ GHz, $\omega_n = -0.5$ MHz, $\gamma_e = 0.5$ GHz, $q_0 = 0.3$, $\phi = -\pi/2$, $\nu_Q = 2.8$ MHz, $\theta = 0$.

alytical solution in the $I = 1/2$ case, Eq. (29), where it is evident that $P(m)$ depends inversely on the flip rates. In Fig. 7, we see that this also occurs for $I > 1/2$. For all values of I, we can physically understand the formation of probability peaks at flip-rate zeros as resulting from the fact that, at these magnetization values, the joint electron-nuclear spin evolution under the HF interaction becomes commensurate with the driving pulses. Consequently, the pulses do not cause a net polarization transfer between the electron and nuclear spins. Thus, these values of the magnetization m provide a point of stability in the electron-nuclear feedback mechanism. We also see from Fig. 7(a), and to some degree from Fig. 7(b), that the polarization distribution is suppressed in the vicinity of $m = -\omega_{e0}/A$ (which corresponds to $m = -10$ for the parameters used in the figure). This is due to the fact that the flip rates are largest near these magnetization values and therefore drive population away from these values.

Another striking feature of the polarization distributions in Fig. 7 is that the distributions for $I > 1/2$ exhibit broad envelopes in addition to the mode-locking peaks. This is a consequence of the fact that there are multiple distinct flip rates for $I > 1/2$, as shown in Eqs. (19) and (21). These flip rates oscillate with ω_e at distinct frequencies that differ from each other by an amount proportional to A. Therefore, they do not all vanish at the same values of ω_e, dulling the sharpness of the mode-locking peaks. This effect becomes diminished at larger N, because in this limit A decreases, and all the flip-rate zeros approach the values of m at which $\omega_{e0} + Am = 2\pi p/T_R$, where p is an integer, producing a more comb-like distribution. The broadening of the distribution at smaller values of N is an important feature that is missed when $I = 1/2$ spins are used to model $I > 1/2$ spin baths. In the example of Fig. 7, we see that it also leads to an increase in the average magnetization $\langle m \rangle$ due to the enhanced weight of the distribution at positive magnetizations. This enhancement is more pronounced for $I = 3/2$ compared to $I = 1$. Fig. 8 examines the behavior of $\langle m \rangle$ as a function of N. The points are obtained by solving the respective kinetic equations, Eqs. (32) and (38). In the $I = 1$ case, it is possible to obtain results for much larger bath sizes because the $\mathcal{R}$ matrix is much smaller in this case. For both $I = 1$ and $I = 3/2$, the points are well described by a linear relationship between $\langle m \rangle$ and N, as shown in the figure. We find that for the parameters considered and for large N, the average polarization for $I = 3/2$ is approximately two times larger compared to that of an $I = 1$ bath, with the net polarization in this case approaching 9%.

The effects of nonzero quadrupolar angle on the polarization distribution for $I = 1, 3/2$ are illustrated in Fig. 9. Here, we set $N = 150$, because nonzero θ reduces the sparsity of the $\mathcal{R}$ matrix, making the numerical computation more intensive than before, especially for $I = 3/2$. From Fig. 9(a), we see that for $I = 1$, nonzero θ leads to quantitative changes in the heights of the mode-locking peaks, along with a slight redistribution of the probability to negative magnetizations for intermediate values

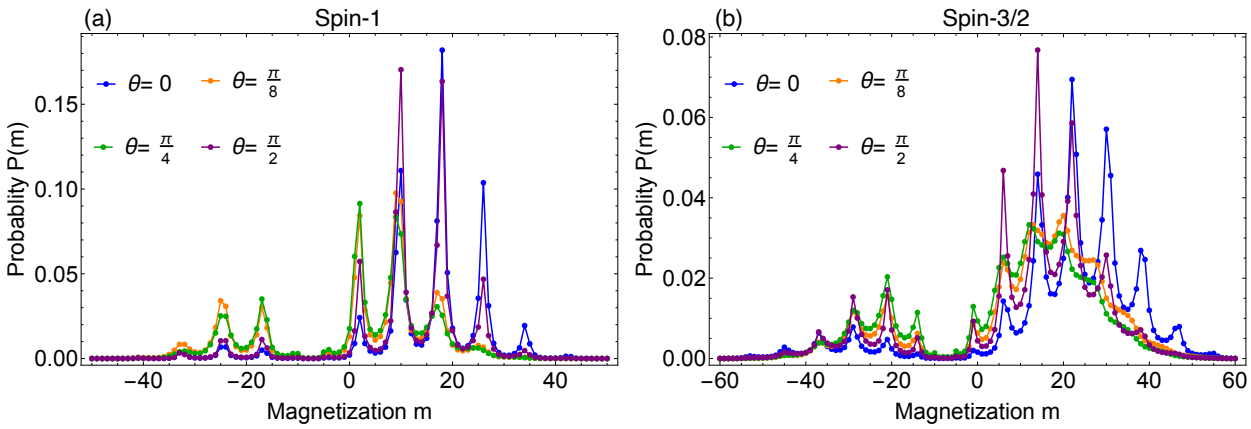

FIG. 9. Steady-state nuclear spin polarization distribution of a bath with $N = 150$ nuclear spins for four different values of the quadrupolar angle θ for (a) $I = 1$ and (b) $I = 3/2$. The parameter values are $T_R = 13.2$ ns, $NA = 10$ GHz, $\omega_{e0} = 0.5$ GHz, $\omega_n = -0.5$ MHz, $\gamma_e = 0.5$ GHz, $q_0 = 0.3$, $\phi = -\pi/2$, $\nu_Q = 2.8$ MHz.

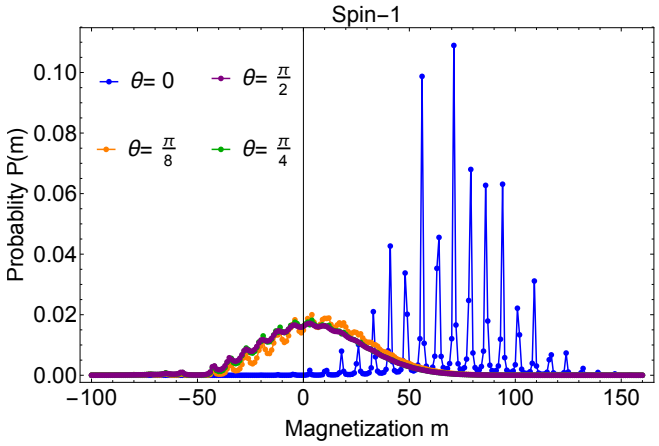

FIG. 10. Steady-state nuclear spin polarization distribution of a bath with $N = 1000$ $I = 1$ nuclear spins for four different values of the quadrupolar angle θ. The other parameter values are $T_R = 13.2$ ns, $NA = 10$ GHz, $\omega_{e0} = 0.5$ GHz, $\omega_n = -0.5$ MHz, $\gamma_e = 0.5$ GHz, $q_0 = 0.3$, $\phi = -\pi/2$, $\nu_Q = 2.8$ MHz.

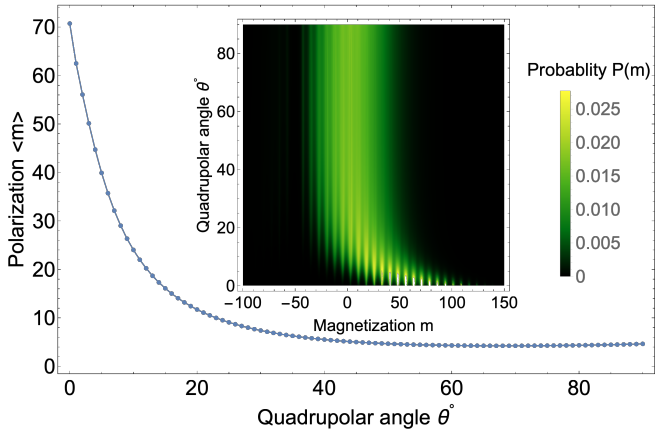

FIG. 11. The average polarization $\langle m \rangle$ of a nuclear spin bath with $N = 1000$ nuclei of total spin $I = 1$ for several values of the quadrupolar angle in the range of $0 \leq \theta \leq \pi/2$. The inset color map shows the steady-state nuclear spin polarization distribution over the same range of quadrupolar angles. The other parameter values are $T_R = 13.2$ ns, $NA = 10$ GHz, $\omega_{e0} = 0.5$ GHz, $\omega_n = -0.5$ MHz, $\gamma_e = 0.5$ GHz, $q_0 = 0.3$, $\phi = -\pi/2$, $\nu_Q = 2.8$ MHz.

of θ. Similar behavior occurs for $I = 3/2$, as shown in Fig. 9(b). The redistribution can be understood from the fact that, in the absence of the HF interaction, the quadrupolar coupling produces a Gaussian distribution centered around $m = 0$. This is discussed in more detail below. The fact that this redistribution is strongest near $\theta = \pi/4$ suggests that the $\Delta m_I = \pm 1$ quadrupolar-driven transitions play an important role in this process. This effect constitutes another way in which the quadrupolar interaction can make the DNP process for $I > 1/2$ depart significantly from what is predicted for an $I = 1/2$ bath. Also notice that in both panels of Fig. 9, the polarization distributions are still suppressed near $m = -\omega_{e0}/A$ even for $\theta > 0$. This indicates that the HF contributions to the flip rates remain an important factor in shaping the overall distribution.

Fig. 10 again shows the effect of nonzero θ for $I = 1$, but now for a bath of size $N = 1000$. For $\theta = 0$, there is a distinct comb-like structure that is the hallmark of mode-locking. However, for $\theta > 0$, this structure quickly disappears and is replaced by an almost Gaussian distribution centered around zero magnetization. A Gaussian distribution is in fact what occurs in the absence of the HF interaction, because the flip rates are then purely due to the quadrupolar coupling, which means that they are independent of m and are equal for $\Delta m_I > 0$ and $\Delta m_I < 0$. This shows that the quadrupolar interaction plays a much more important role compared to the HF interaction for the case considered in Fig. 10. This is

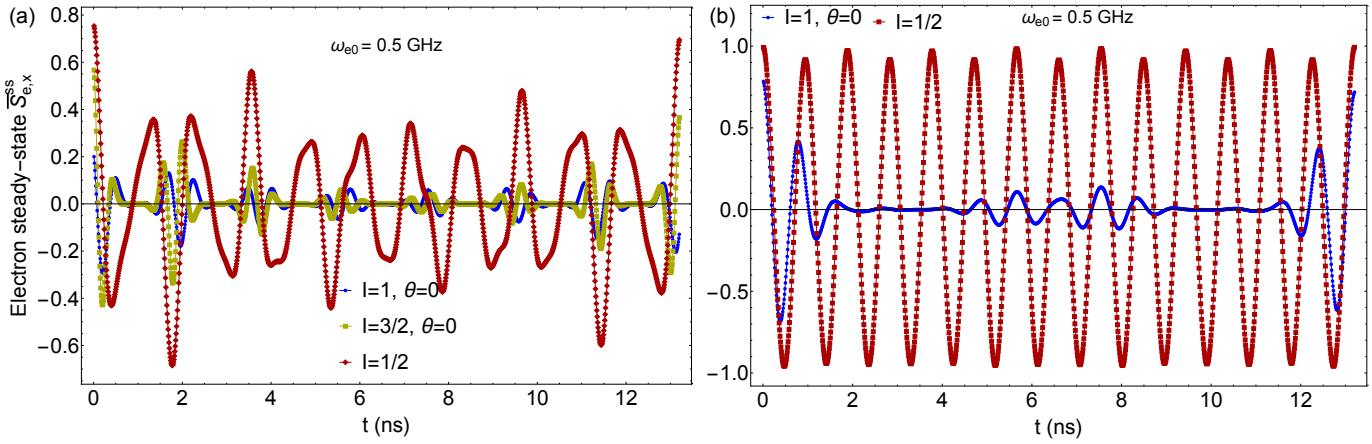

FIG. 12. The feedback effect of nuclear spin polarization on the x component of the electron spin steady state as a function of time over one drive period $T_R = 13.2$ ns. (a) $N = 150$ nuclei of spin $I = 1/2, 1$ and $3/2$, and (b) $N = 1000$ nuclei of spin $I = 1/2$ and 1. The parameter values are $NA = 10$ GHz, $\omega_n = -0.5$ MHz, $\gamma_e = 0.5$ GHz, $q_0 = 0.3$, $\phi = -\pi/2$, $\nu_Q = 2.8$ MHz.

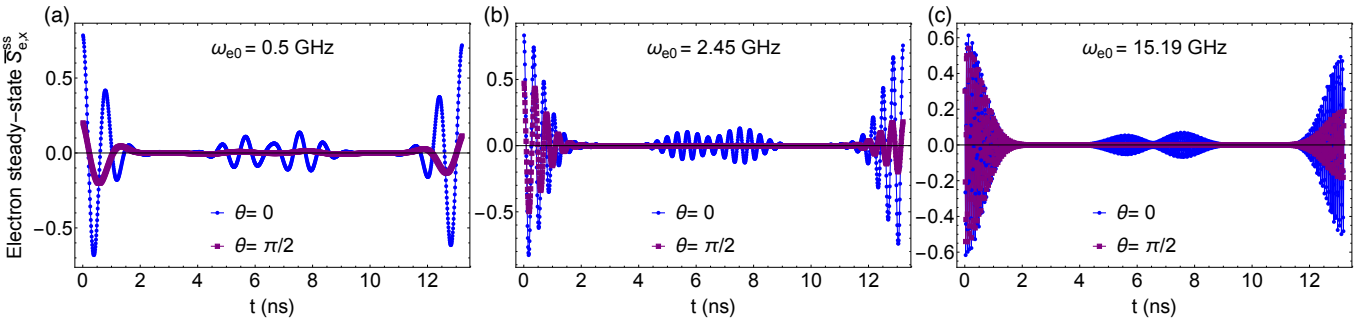

FIG. 13. The feedback effect of $N = 1000$ $I = 1$ nuclear spins on the x component of the electron spin steady state as a function of time over one drive period $T_R = 13.2$ ns. Here the quadrupolar angles $\theta = 0$ and $\theta = \pi/2$ are considered for different bare electron Zeeman frequencies of (a) 0.5 GHz, (b) 2.45 GHz and (c) 15.19 GHz. The electron Zeeman frequencies chosen for (b) and (c) correspond to the local minima shown in Fig. 14 and the nuclear spin polarization distribution for (a) is shown in Fig. 10. The parameter values are $NA = 10$ GHz, $\omega_n = -0.5$ MHz, $\gamma_e = 0.5$ GHz, $q_0 = 0.3$, $\phi = -\pi/2$, $\nu_Q = 2.8$ MHz.

because the larger value of N corresponds to a reduction in the HF coupling A, and hence in the magnitude of the flip rates (see Eq. (19)). This in turn increases the relative importance of the quadrupolar interaction. This can be seen from Fig. 4, where it is evident that as θ increases, the flip rate for the $\Delta m_I = 2$ transition quickly surpasses the difference in the flip rates for the $\Delta m_I = \pm 1$ transitions. As a consequence, the probability distribution is no longer sensitive to the detailed features of the $\Delta m_I = \pm 1$ transitions, which are responsible for both the comb-like mode-locking structure and the suppression near $m = -\omega_{e0}/A$. This shows that even small values of θ can have a dramatic effect on the DNP process for large numbers of nuclei. This is quantified in Fig. 11, which shows how the nuclear spin polarization distribution and average magnetization, $\langle m \rangle$, depend on θ. The latter quickly decays with increasing θ. As is evident from the inset in Fig. 11, the distribution itself exhibits mode-locking fringes at small θ that become blurred at larger θ. The sensitivity of mode-locking to the quadrupolar interaction suggests that it could be used as a diagnostic tool to estimate the quadrupolar coupling strength and angle in experiments. This is further supported in the next section, where we show how the steady-state electron spin vector in the presence of DNP feedback depends on the quadrupolar angle.

B. Feedback on electron spin

Once we obtain the steady-state polarization distribution of the nuclear spin bath, the final step is to update the steady state of the electron by applying the Overhauser shift to the Zeeman frequency:

$$\overline{S}^{ss}_{e,i}(t, \omega_{e0}) = \sum_m P(m) S^{ss}_{e,i}(t, \omega_{e0} + mA). \qquad (44)$$

Here the summation is over all possible values of m, and t is the time elapsed since the last pulse. We obtain the time-evolved electron steady state by starting from the expression for the steady state immediately after a pulse, Eq. (B5), and evolving it under Larmor precession with

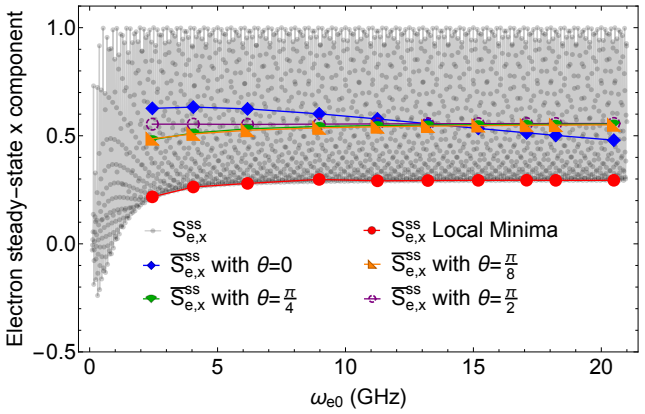

FIG. 14. The effect of the $I = 3/2$ nuclear feedback on the x component of the steady-state electron spin vector. The red filled circles indicate local minima of $S^{ss}_{e,x}$ (shown in gray) for several values of the electron Zeeman frequency ω_{e0} without nuclear feedback. The other points indicate the values of $\overline{S}^{ss}_{e,x}(\omega_{e0})$ at the same values of ω_{e0}, but now with feedback included as in Eq. (44). Results for four different values of the quadrupolar angle θ are shown. Other parameter values are $N = 150$, $T_R = 13.2$ ns, $NA = 10$ GHz, $\omega_n = -0.5$ MHz, $\gamma_e = 0.5$ GHz, $q_0 = 0.3$, $\phi = -\pi/2$, $\nu_Q = 2.8$ MHz.

frequency $\omega_{e0}+mA$ for time t. Fig. 12 shows the resulting DNP-modified electron steady state over one drive period for different species of nuclear spins. Fig. 12(a) compares $I = 1/2$, 1 and 3/2 species for $N = 150$, where the two latter DNP distributions are shown in Fig. 9 for $\theta = 0$. Fig. 12(b) compares the cases $I = 1/2$ and 1 for $N = 1000$. It is evident that the total spin of the nuclei can have a significant effect on the electron spin precession in the steady state. Because the mode-locking effect is stronger in the spin 1/2 case (see Fig. 7), the electron spin precession is closer to a sinusoid due to the fact that only a few discrete values of the Overhauser field contribute to the sum in Eq. (44). On the other hand, for larger spin, the nuclear polarization distribution is broader, giving rise to a beating in the electron spin vector over each driving period.

The role of quadrupolar interactions in the feedback is examined in Fig. 13, which shows the resulting DNP-modified electron steady state over one drive period for six different $N = 1000$, $I = 1$ polarization distributions. Two of these are distributions shown in Fig. 10—the ones corresponding to $\theta = 0$ and $\theta = \pi/2$. The modified steady states for these two cases are shown in Fig. 13(a), where it is evident that a large quadrupolar angle suppresses oscillations, both in the vicinity of the driving pulses and in the "echo" that occurs in the middle of the drive period near $t = T_R/2$, which is 6.6 ns for the chosen parameter values. Similar behavior occurs for other values of the external magnetic field, as is demonstrated in Figs. 13(b), (c). It should be noted that the amplitude of these oscillations are used to identify the presence of mode-locking [52–58], and so the suppression of these oscillations can provide an experimental indicator of substantial quadrupolar effects.

The electron steady state, Eq. (B5), is a rapidly oscillatory function of the applied magnetic field. In Ref. [73], it was found using perturbation theory that for $I = 1/2$, nuclear feedback suppresses the amplitudes of these oscillations. In particular, it was shown that the x component of the electron steady-state SV approaches unity for all values of the external magnetic field as a consequence of mode-locking: The SV becomes synchronized with the pulses such that it lies parallel to the optical axis at the pulse times. Here, we examine how this effect is modified by the presence of quadrupolar interactions. This is illustrated in the case of $I = 3/2$ in Fig. 14, where we show the x-component of the electron steady state immediately after a pulse, $S^{ss}_{e,x}$, for ten different values of the electron Zeeman frequency with and without feedback. We are primarily interested in the amplitude of the electron steady-state oscillations, so we choose the ten different Zeeman frequencies that correspond to minima of the oscillations in the absence of feedback (red dots in Fig. 14). To find how the envelope of the electron spin oscillations is affected by the feedback process, we compute the nuclear spin polarization distributions for each of these minima. These distributions then alter the values of these minima according to Eq. (44) (with $t = 0$). As can be seen from Fig. 14, the amplitude of the electron steady-state oscillations is suppressed (i.e., the minima increase up toward unity) in the presence of DNP, and the degree of this suppression varies weakly and nonmonotonically with the quadrupolar angle θ. To understand this behavior better, in Fig. 15 we show the polarization distributions for five of the minima from Fig. 14 for four different quadrupolar angles. It is clear that for all values of θ, as the electron spin Zeeman frequency due to the external magnetic field, ω_{e0}, is increased, the polarization distributions gravitate toward $m = 0$. This is because larger values of the electron Zeeman frequency suppress HF flip-flops, as the violation of energy conservation becomes more pronounced in this case. This is why the $\theta = 0$ curve in Fig. 14 monotonically decreases with increasing ω_{e0}. On the other hand, quadrupole-induced nuclear spin flips do not depend on the electron Zeeman frequency, and so these gradually begin to dominate as both θ and ω_{e0} increase. This in turn causes the curves in Fig. 14 to become essentially independent of ω_{e0} as θ increases. This is another manifestation of how quadrupolar interactions suppress mode-locking effects.

V. CONCLUSIONS

In this work, we developed a general theoretical framework to describe the dynamics of an electron trapped in a self-assembled quantum dot that is driven by a periodic train of optical pulses and coupled to a nuclear spin bath. Using a dynamical, self-consistent, mean-field type approach, we calculated the steady-state dynamic nuclear polarization, as well as its influence on the evolution of

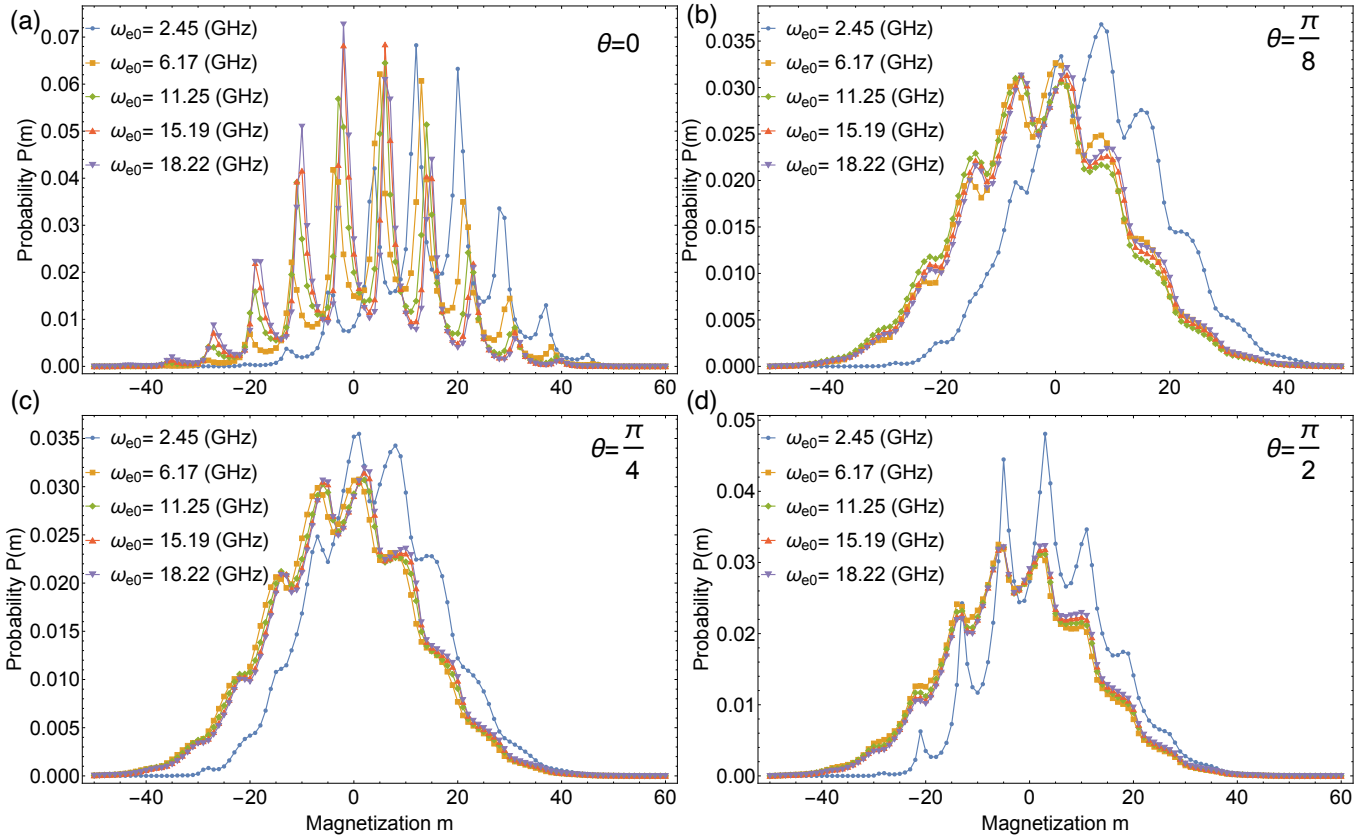

FIG. 15. The nuclear spin polarization distributions corresponding to five of the electron Zeeman frequency values from Fig. 14 for quadrupolar angles (a) $\theta = 0$, (b) $\theta = \pi/8$, (c) $\theta = \pi/4$, and (d) $\theta = \pi/2$ for an $I = 3/2$ nuclear bath. Other parameter values are $N = 150$, $T_R = 13.2$ ns, $NA = 10$ GHz, $\omega_n = -0.5$ MHz, $\gamma_e = 0.5$ GHz, $q_0 = 0.3$, $\phi = -\pi/2$, $\nu_Q = 2.8$ MHz.

the electron spin. Our framework is non-perturbative, applies to nuclei of arbitrary total spin I, and includes quadrupolar effects that arise for $I > 1/2$.

We showed that the phenomenon of mode-locking, or DNP-induced frequency-focusing, seen in experiments [52–58] emerges naturally from our formalism. It can be understood as originating from the structure of the rates for the electron and nuclear spins to flip with one another under the hyperfine interaction. The flip rates vanish when the effective electron precession frequency (including the DNP-driven Overhauser shift) becomes commensurate with the optical pulse train, because in this case the pulses do not interrupt the joint electron-nuclear evolution, and so no polarization is transferred from the electron spin to the nuclei. The vanishing of the flip rates then leads to sharp peaks in the nuclear polarization distribution at magnetization values that satisfy the commensurability condition. Our exact result for the nuclear spin probability distribution in the $I = 1/2$ case makes this connection explicit, since the distribution depends inversely on the flip rates. In addition to mode-locking, we showed that hyperfine flip-flops also give rise to a net nuclear spin polarization that appears to grow linearly with the number of nuclei.

It is worth considering how the mode-locking peaks determined by the commensurability condition (Eq. (30)) might be modified if we were to go beyond the box model and include a distribution of hyperfine couplings. First we note that, for generic choices of the applied magnetic field, only the nuclei that are closest to the center of the electronic wavefunction contribute to mode-locking. This is because $P(m)$ is concentrated near relatively small values of m (for $I = 1/2$ this is due to the Gaussian-like factor in Eq. (29)), so the smallness of the hyperfine couplings of the nuclei that are farther away cannot be compensated by larger values of m to satisfy the commensurability condition. Small variations in the hyperfine couplings of nuclei close to the center could be incorporated using a "wedding cake" model in which the nuclei are separated into groupings defined by distinct values of the hyperfine coupling. These groupings could be treated as smaller, independent spin baths, each with its own mode-locking condition. Distinct but nearly-equal values of A will give rise to mode-locking peaks at almost the same magnetization values m, and collectively these closely-spaced peaks will form broader mode-locking features in $P(m)$. The fact that clear signatures of frequency-focusing are seen in experiments [52–58] suggests that this broadening is a relatively small effect.

Our formalism includes not only hyperfine-driven phe-

nomena, but also quadrupolar effects that can arise for $I > 1/2$. We found that the importance of quadrupolar interactions depends sensitively on the quadrupolar angle θ between the applied magnetic field and the principal axis of strain in the dot. For $\theta < \pi/8$, hyperfine interactions tend to dominate, leading to clear signatures of mode-locking. However, for $\theta \geq \pi/8$, quadrupole-induced nuclear spin flips begin to dominate, which leads to a suppression of mode-locking and a reduction of the net nuclear polarization. We also showed that quadrupolar effects become more pronounced when the applied magnetic field is increased, because hyperfine flip-flops are suppressed by the increasingly large Zeeman energy mismatch between the electron and nuclei. These effects are clearly visible in the nuclear spin polarization distributions for both $I = 1$ and $I = 3/2$, and they translate to experimentally detectable signatures that are encoded in the presence or absence of electron spin oscillations in the steady state. Hyperfine flip-flops lead to coherent oscillations in the vicinity of each pulse and halfway between pulses, while quadrupolar interactions act to suppress these oscillations. These signatures offer a potential method to measure the strength of quadrupolar interactions in quantum dots.

The framework we have presented constitutes an efficient, quantitative approach to describing the dynamics of a driven spin coupled to a spin bath. Going forward, it would be interesting to see if some of the simplifying assumptions made here can be relaxed to enhance quantitative accuracy. For example, can we go beyond the box model limit and allow for non-uniform hyperfine couplings, perhaps using a "wedding cake" model in which the electronic wavefunction envelope is approximated by a piecewise-constant function? Such a generalization would also allow for the inclusion of multiple nuclear species, which is relevant for common semiconductor QD compounds such as InGaAs. It would also be interesting to extend this method beyond the independent nuclei approximation, perhaps using a cluster-based approach in which inter-nuclear interactions are included gradually within clusters of increasing size [20, 114]. In terms of applications, our framework could be employed to design driving protocols to achieve desired bath polarization states to either mitigate decoherence or utilize the bath as a quantum memory [89–92]. Finally, we note that the theory we developed is quite general and could be applied to other problems involving a driven system coupled to a quantum bath.

ACKNOWLEDGEMENTS

EB acknowledges support from NSF Grant No. 1847078. SEE acknowledges support from NSF Grant No. 1839056.

Appendix A: Kraus operators for optical pumping of the electron

The existence of a hierarchy of timescales in mode-locking experiments allows us to first solve for the electron spin dynamics without having to include nuclear spin effects. This is due to the fact that the nuclear spin dynamics are slow compared to those of the electron. Given that the nuclear spins are the main source of decoherence for the electron, this means we can also neglect electron spin decoherence effects. In addition, the optical pumping and spontaneous emission are fast compared to the pulse period, $\gamma_e T_R \gg 1$, which ensures that the excited population returns fully to the ground state before the next pulse comes. This allows us to treat the evolution of the electron over each period in terms of a dynamical map that acts only on the electron spin ground state subspace, as in Eq. (7).

The Kraus operators, E_k, that make up the dynamical map can be found by explicitly computing the non-unitary part of the evolution for an arbitrary initial density matrix and comparing the initial and final density matrices [73]. To compute the non-unitary part of the evolution due to the sequence of pulses $H_c(t)$, we only need the electronic parts of the full Hamiltonian in Eq. (1): $H_e(t) = H_{0,e} + H_c(t)$. The fact that the pulse is much shorter than the spin precession period allows us to ignore the precession during the action of the pulse. Therefore $|\bar{x}\rangle$ and $|\bar{T}\rangle$ can be considered as an effective two-level system, where the evolution operator due to the pulse in the $|x\rangle$, $|\bar{x}\rangle$, $|\bar{T}\rangle$ basis is

$$U_p = \begin{bmatrix} 1 & 0 & 0 \\ 0 & u_{\bar{x}\bar{x}} & -u^*_{\bar{T}\bar{x}} \\ 0 & u_{\bar{T}\bar{x}} & u^*_{\bar{x}\bar{x}} \end{bmatrix}. \tag{A1}$$

After the pulse, a fraction $|u_{\bar{T}\bar{x}}|^2$ of the population remains in the trion state. We can describe the decay of this population due to spontaneous emission using the Liouville-von Neumann equation with appropriately chosen Lindblad operators $\mathcal{L}$: $\dot{\rho} = i[\rho, H_{0,e}] + \mathcal{L}(\rho)$, where the first term includes the Larmor precession of the ground spin states during the decay. Solving this equation for an arbitrary initial state then yields the following Kraus operators in the $|x\rangle$, $|\bar{x}\rangle$ basis [73]:

$$E_1 = \begin{bmatrix} 1 & 0 \\ 0 & q \end{bmatrix}, \quad E_2 = \begin{bmatrix} 0 & a_1 \\ 0 & -a_2 \end{bmatrix}, \quad E_3 = \begin{bmatrix} 0 & 0 \\ 0 & \kappa \end{bmatrix}, \tag{A2}$$

where $q = u_{\bar{x}\bar{x}} \equiv q_o e^{i\phi}$, $a_1 = \omega_e \sqrt{(1-q_o^2)/2(4\gamma_e^2 + \omega_e^2)}$, $a_2 = i\gamma_e \sqrt{2}\sqrt{(1-q_o^2)/(4\gamma_e^2+\omega_e^2)}$, and $\kappa = \sqrt{1 - q_o^2 - a_1^2 - |a_2|^2}$. These Kraus operators guarantee the unity of the trace of the density matrix by satisfying $\sum_k E_k^\dagger E_k = \mathbb{1}$. The parameter q_o quantifies the amount of population remaining in the spin state $|\bar{x}\rangle$ after the pulse is applied, and ϕ is the angle about the x axis by which the pulse rotates the electron spin. These two parameters can be computed given a specific pulse

shape, but in the following we leave these parameters arbitrary. Note that these Kraus operators capture the evolution of the electronic spin from the beginning of the pulse until a steady state is reached under the combined action of precession and spontaneous emission. This steady state is reached on timescales large compared to $1/\gamma_e$.

Appendix B: Electron spin steady state

We can use the Kraus operators from above to compute the electron spin steady state. Rather than work directly with the Kraus operators, it is more convenient to switch to the spin vector (SV) representation, especially since finding the steady state requires applying the Kraus operators an infinite number of times. In general, a SV S transforms under non-unitary evolution as follows:

$$S' = YS + K, \tag{B1}$$

where Y is a matrix that generally both rotates and shrinks the SV, while K corresponds to the non-unital part of the evolution (i.e., a loss or gain of population in the subspace described by S). If K is nonzero, then a nontrivial steady state is possible. As shown in Ref. [73], for spin 1/2 these quantities can be obtained from the Kraus operators using the following formulas:

$$K_i = \frac{1}{2}\mathrm{Tr}\sum_k \hat{\sigma}_i \mathcal{E}_k \mathcal{E}_k^\dagger, \tag{B2}$$

$$Y_{ij} = \frac{1}{2}\mathrm{Tr}\sum_k \hat{\sigma}_i \mathcal{E}_k \hat{\sigma}_j \mathcal{E}_k^\dagger, \tag{B3}$$

where the $\hat{\sigma}_i$ are Pauli matrices. In the case of the mode-locking experiment, the Kraus operators $\mathcal{E}_k$ evolve the electron spin over one period, that is, they include both the non-unitary dynamics (E_k) generated by a pulse and also the unitary precession under the magnetic field over time T_R: $\mathcal{E}_k = E_k e^{-i\omega_e T_R \hat{S}_z}$. In concatenating these two parts of the evolution in this way, we are assuming that the drive period is much longer than the time it takes the electron to reach a steady state following the pulse. This in turn requires $T_R\gamma_e \gg 1$, which is typically satisfied in mode-locking experiments [52–58]. To find the steady state, it is convenient to combine both Y and K into a single 4×4 matrix:

$$\mathcal{Y}_e = \begin{bmatrix} 1 & 0 & 0 & 0 \\ K_x & Y_{xx} & Y_{xy} & Y_{xz} \\ K_y & Y_{yx} & Y_{yy} & Y_{yz} \\ K_z & Y_{zx} & Y_{zy} & Y_{zz} \end{bmatrix}, \tag{B4}$$

where the evolution of the electron SV over one period is now given by $\mathcal{S}_e' = \mathcal{Y}_e\mathcal{S}_e$. Here, the first component of the 4-component SV $\mathcal{S}_e$ is always fixed to 1, while the remaining three components constitute the usual spin 1/2 SV. In this representation it is easy to see that the steady state $\mathcal{S}_e^{ss} = (1, S_{e,x}^{ss}, S_{e,y}^{ss}, S_{e,z}^{ss})$ is the eigenvector of $\mathbb{1}-\mathcal{Y}_e$ with eigenvalue zero. Transforming the Kraus operators of Eq. (A2) from the x basis to the z basis, plugging the result into Eq. (B4), and computing the null vector of $\mathcal{Y}_e$ leads to the following steady state electron SV [73]:

$$\begin{aligned}
S_{e,x}^{ss} &= \frac{a_1\left(a_1 q_o\left(q_o-\cos\phi\right)\cos\left(\omega_e T_R\right) - i a_2\left(q_o\cos\phi-1\right)\sin\left(\omega_e T_R\right) - a_1 q_o\cos\phi + a_1\right)}{\left(a_1^2+q_o^2-1\right)\cos\left(\omega_e T_R\right) - a_1 q_o\cos\phi\left[i a_2\sin\left(\omega_e T_R\right) + a_1\cos\left(\omega_e T_R\right) + a_1\right] + i a_1 a_2\sin\left(\omega_e T_R\right) + \left(a_1^2-1\right)q_o^2 + 1}, \\
S_{e,y}^{ss} &= \frac{a_1\left(a_1 q_o\left(\cos\phi-q_o\right)\sin\left(\omega_e T_R\right) - i a_2\left(q_o\cos\phi-1\right)\left(\cos\left(\omega_e T_R\right)-1\right)\right)}{\left(a_1^2+q_o^2-1\right)\cos\left(\omega_e T_R\right) - a_1 q_o\cos\phi\left[i a_2\sin\left(\omega_e T_R\right) + a_1\cos\left(\omega_e T_R\right) + a_1\right] + i a_1 a_2\sin\left(\omega_e T_R\right) + \left(a_1^2-1\right)q_o^2 + 1}, \\
S_{e,z}^{ss} &= \frac{a_1 q_o\sin\phi\left(a_1\sin\left(\omega_e T_R\right) - i a_2\left(\cos\left(\omega_e T_R\right)-1\right)\right)}{\left(a_1^2+q_o^2-1\right)\cos\left(\omega_e T_R\right) - a_1 q_o\cos\phi\left[i a_2\sin\left(\omega_e T_R\right) + a_1\cos\left(\omega_e T_R\right) + a_1\right] + i a_1 a_2\sin\left(\omega_e T_R\right) + \left(a_1^2-1\right)q_o^2 + 1}.
\end{aligned} \tag{B5}$$

These are the components of the electron SV immediately after each pulse. The steady state at other times during the driving period can be obtained by rotating this vector about the z axis by angle $\omega_e T_R$ (to account for the Larmor precession).

[1] T. D. Ladd, F. Jelezko, R. Laflamme, Y. Nakamura, C. Monroe, and J. L. OBrien, "Quantum computers," Nature **464**, 4553 (2010).

[2] Ren-Bao Liu, Wang Yao, and L. J. Sham, "Quantum computing by optical control of electron spins," Advances in Physics **59**, 703–802 (2010).

[3] Nikolai Lauk, Neil Sinclair, Shabir Barzanjeh, Jacob P Covey, Mark Saffman, Maria Spiropulu, and Christoph

Simon, "Perspectives on quantum transduction," Quantum Science and Technology **5**, 020501 (2020).
[4] Stephanie Wehner, David Elkouss, and Ronald Hanson, "Quantum internet: A vision for the road ahead," Science **362** (2018), 10.1126/science.aam9288.
[5] Sophia E. Economou, L. J. Sham, Yanwen Wu, and D. G. Steel, "Proposal for optical u(1) rotations of electron spin trapped in a quantum dot," Phys. Rev. B **74**, 205415 (2006).
[6] A. Greilich, Sophia E. Economou, S. Spatzek, D. R. Yakovlev, D. Reuter, A. D. Wieck, T. L. Reinecke, and M. Bayer, "Ultrafast optical rotations of electron spins in quantum dots," Nature Physics **5**, 262266 (2009).
[7] M Makhonin, K. Kavokin, P. Senellart, Aristide Lematre, M Skolnick, and Alexander Tartakovskii, "Fast control of nuclear spin polarization in an optically pumped single quantum dot," Nature materials **10**, 844–8 (2011).
[8] Xing Ding, Yu He, Z.-C. Duan, Niels Gregersen, M.-C. Chen, S. Unsleber, S. Maier, Christian Schneider, Martin Kamp, Sven Höfling, Chao-Yang Lu, and Jian-Wei Pan, "On-demand single photons with high extraction efficiency and near-unity indistinguishability from a resonantly driven quantum dot in a micropillar," Phys. Rev. Lett. **116**, 020401 (2016).
[9] Sonia Buckley, Kelley Rivoire, and Jelena Vukovi, "Engineered quantum dot single-photon sources," Reports on Progress in Physics **75**, 126503 (2012).
[10] Yu-Jia Wei, Yu-Ming He, Ming-cheng Chen, Yi-Nan Hu, Yu He, Dian Wu, Christian Schneider, M. Kamp, Sven Hfling, Chao-Yang Lu, and Jian-Wei Pan, "Deterministic and robust generation of single photons from a single quantum dot with 99.5% indistinguishability using adiabatic rapid passage," Nano Letters **14**, 6515 (2014).
[11] Pascale Senellart, Glenn Solomon, and Andrew White, "High-performance semiconductor quantum-dot single-photon sources," Nature Nanotechnology **12**, 1026–1039 (2017).
[12] Netanel H. Lindner and Terry Rudolph, "Proposal for pulsed on-demand sources of photonic cluster state strings," Phys. Rev. Lett. **103**, 113602 (2009).
[13] Donovan Buterakos, Edwin Barnes, and Sophia E. Economou, "Deterministic generation of all-photonic quantum repeaters from solid-state emitters," Phys. Rev. X **7**, 041023 (2017).
[14] Antonio Russo, Edwin Barnes, and Sophia E. Economou, "Photonic graph state generation from quantum dots and color centers for quantum communications," Phys. Rev. B **98**, 085303 (2018).
[15] Paul Hilaire, Edwin Barnes, and Sophia E. Economou, "Resource requirements for efficient quantum communication using all-photonic graph states generated from a few matter qubits," (2020), arXiv:2005.07198 [quant-ph].
[16] I. Schwartz, D. Cogan, E. R. Schmidgall, Y. Don, L. Gantz, O. Kenneth, N. H. Lindner, and D. Gershoni, "Deterministic generation of a cluster state of entangled photons," Science **354**, 434437 (2016).
[17] Bernhard Urbaszek, Xavier Marie, Thierry Amand, Olivier Krebs, Paul Voisin, Patrick Maletinsky, Alexander Högele, and Atac Imamoglu, "Nuclear spin physics in quantum dots: An optical investigation," Rev. Mod. Phys. **85**, 79–133 (2013).
[18] Chia-Wei Huang and Xuedong Hu, "Theoretical study of nuclear spin polarization and depolarization in self-assembled quantum dots," Phys. Rev. B **81**, 205304 (2010).
[19] I. A. Merkulov, Al. L. Efros, and M. Rosen, "Electron spin relaxation by nuclei in semiconductor quantum dots," Phys. Rev. B **65**, 205309 (2002).
[20] Wang Yao, Ren-Bao Liu, and L. J. Sham, "Theory of electron spin decoherence by interacting nuclear spins in a quantum dot," Phys. Rev. B **74**, 195301 (2006).
[21] Robert Stockill, C. Gall, Clemens Matthiesen, L. Huthmacher, E. Clarke, M. Hugues, and Mete Atatre, "Quantum dot spin coherence governed by a strained nuclear environment," Nature Communications **7**, 12745 (2016).
[22] W. A. Coish and Daniel Loss, "Hyperfine interaction in a quantum dot: Non-markovian electron spin dynamics," Phys. Rev. B **70**, 195340 (2004).
[23] Łukasz Cywiński, Wayne M. Witzel, and S. Das Sarma, "Electron spin dephasing due to hyperfine interactions with a nuclear spin bath," Phys. Rev. Lett. **102**, 057601 (2009).
[24] Łukasz Cywiński, Wayne M. Witzel, and S. Das Sarma, "Pure quantum dephasing of a solid-state electron spin qubit in a large nuclear spin bath coupled by long-range hyperfine-mediated interactions," Phys. Rev. B **79**, 245314 (2009).
[25] Edwin Barnes, Łukasz Cywiński, and S. Das Sarma, "Nonperturbative master equation solution of central spin dephasing dynamics," Phys. Rev. Lett. **109**, 140403 (2012).
[26] Alexander Khaetskii, Daniel Loss, and Leonid Glazman, "Electron spin evolution induced by interaction with nuclei in a quantum dot," Phys. Rev. B **67**, 195329 (2003).
[27] Michael Bortz and Joachim Stolze, "Exact dynamics in the inhomogeneous central-spin model," Phys. Rev. B **76**, 014304 (2007).
[28] D. Gammon, Al. L. Efros, T. A. Kennedy, M. Rosen, D. S. Katzer, D. Park, S. W. Brown, V. L. Korenev, and I. A. Merkulov, "Electron and nuclear spin interactions in the optical spectra of single GaAs quantum dots," Phys. Rev. Lett. **86**, 5176–5179 (2001).
[29] Evgeny Chekhovich, Saimon Covre da Silva, and Armando Rastelli, "Nuclear spin quantum register in an optically active semiconductor quantum dot," Nature Nanotechnology **15**, 1–6 (2020).
[30] D. Gammon, E. S. Snow, B. V. Shanabrook, D. S. Katzer, and D. Park, "Fine structure splitting in the optical spectra of single GaAs quantum dots," Phys. Rev. Lett. **76**, 3005–3008 (1996).
[31] D. Gammon, S. W. Brown, E. S. Snow, T. A. Kennedy, D. S. Katzer, and D. Park, "Nuclear spectroscopy in single quantum dots: Nanoscopic raman scattering and nuclear magnetic resonance," Science **277**, 85–88 (1997).
[32] Evgeny Chekhovich, M Makhonin, Alexander Tartakovskii, Amir Yacoby, H Bluhm, Katja Nowack, and L Vandersypen, "Nuclear spin effects in semiconductor quantum dots," Nature materials **12**, 494–504 (2013).
[33] Gunter Wuest, Mathieu Munsch, Franziska Maier, Andreas Kuhlmann, Arne Ludwig, Andreas Wieck, Daniel Loss, Martino Poggio, and Richard Warburton, "Role of the electron spin in determining the coherence of the nuclear spins in a quantum dot," Nature Nanotechnol-

ogy **11** (2016), 10.1038/nnano.2016.114.
[34] E. A. Chekhovich, M. N. Makhonin, K. V. Kavokin, A. B. Krysa, M. S. Skolnick, and A. I. Tartakovskii, "Pumping of nuclear spins by optical excitation of spin-forbidden transitions in a quantum dot," Phys. Rev. Lett. **104**, 066804 (2010).
[35] Thaddeus D. Ladd, David Press, Kristiaan De Greve, Peter L. McMahon, Benedikt Friess, Christian Schneider, Martin Kamp, Sven Höfling, Alfred Forchel, and Yoshihisa Yamamoto, "Pulsed nuclear pumping and spin diffusion in a single charged quantum dot," Phys. Rev. Lett. **105**, 107401 (2010).
[36] Ivo T. Vink, Katja C. Nowack, Frank H. L. Koppens, Jeroen Danon, Yuli V. Nazarov, and Lieven M. K. Vandersypen, "Locking electron spins into magnetic resonance by electronnuclear feedback," Nature Physics **5**, 764768 (2009).
[37] W. Beugeling, Götz S. Uhrig, and Frithjof B. Anders, "Quantum model for mode locking in pulsed semiconductor quantum dots," Phys. Rev. B **94**, 245308 (2016).
[38] Erik Welander, Evgeny Chekhovich, Alexander Tartakovskii, and Guido Burkard, "Influence of nuclear quadrupole moments on electron spin coherence in semiconductor quantum dots," (2014), arXiv:1405.1329 [cond-mat.mes-hall].
[39] E.A. Chekhovich, M. Hopkinson, M.S. Skolnick, and A.I. Tartakovskii, "Suppression of nuclear spin bath fluctuations in self-assembled quantum dots induced by inhomogeneous strain," Nature Communications **6** (2015), 10.1038/ncomms7348.
[40] C. Kloeffel, P. A. Dalgarno, B. Urbaszek, B. D. Gerardot, D. Brunner, P. M. Petroff, D. Loss, and R. J. Warburton, "Controlling the interaction of electron and nuclear spins in a tunnel-coupled quantum dot," Phys. Rev. Lett. **106**, 046802 (2011).
[41] Patrick Maletinsky, M. Kroner, and A. Imamoglu, "Breakdown of the nuclear-spin-temperature approach in quantum-dot demagnetization experiments," Nature Physics **5**, 407–411 (2009).
[42] Evgeny Chekhovich, K. Kavokin, Jorge Puebla, Andrey Krysa, M. Hopkinson, A Andreev, A. Sanchez, Richard Beanland, M Skolnick, and Alexander Tartakovskii, "Structural analysis of strained quantum dots using nuclear magnetic resonance," (2012).
[43] O. Krebs, P. Maletinsky, T. Amand, B. Urbaszek, A. Lemaître, P. Voisin, X. Marie, and A. Imamoglu, "Anomalous hanle effect due to optically created transverse overhauser field in single InAs/GaAs quantum dots," Phys. Rev. Lett. **104**, 056603 (2010).
[44] Evgeny Chekhovich, Mikhail Glazov, Andrey Krysa, M. Hopkinson, P. Senellart, Aristide Lematre, Alexander Tartakovskii, and M. Skolnick, "Element-sensitive measurement of the holenuclear spin interaction in quantum dots," Nature Physics **9**, 74 (2013).
[45] A. Greilich, M. Wiemann, F. G. G. Hernandez, D. R. Yakovlev, I. A. Yugova, M. Bayer, A. Shabaev, Al. L. Efros, D. Reuter, and A. D. Wieck, "Robust manipulation of electron spin coherence in an ensemble of singly charged quantum dots," Phys. Rev. B **75**, 233301 (2007).
[46] Mathieu Munsch, Gunter Wuest, Andreas Kuhlmann, Fei Xue, Arne Ludwig, D. Reuter, Andreas Wieck, Martino Poggio, and Richard Warburton, "Erratum: Manipulation of the nuclear spin ensemble in a quantum dot with chirped magnetic resonance pulses," Nature nanotechnology **9**, 671 (2013).
[47] Jonathan Prechtel, Andreas Kuhlmann, Julien Houel, Arne Ludwig, Sascha Valentin, Andreas Wieck, and Richard Warburton, "Decoupling a hole spin qubit from the nuclear spins," Nature Materials **15** (2016), 10.1038/nmat4704.
[48] P. Schering and G. S. Uhrig, "Nuclear magnetic resonance spectroscopy of nonequilibrium steady states in quantum dots," (2020), arXiv:2012.03607 [cond-mat.mes-hall].
[49] J. H. Bodey, R. Stockill, E. V. Denning, D. A. Gangloff, G. thier Majcher, D. M. Jackson, E. Clarke, M. Hugues, C. Le Gall, and M. Atatre, "Optical spin locking of a solid-state qubit," npj Quantum Information **5** (2019), 10.1038/s41534-019-0206-3.
[50] Dorian A. Gangloff, Leon Zaporski, Jonathan H. Bodey, Clara Bachorz, Daniel M. Jackson, Gabriel thier Majcher, Constantin Lang, Edmund Clarke, Maxime Hugues, Claire Le Gall, and Mete Atatre, "Revealing beyond-mean-field correlations in a nuclear ensemble via a proxy qubit," (2020), arXiv:2012.11279 [cond-mat.mes-hall].
[51] Aaron M. Ross, Allan S. Bracker, Michael K. Yakes, Daniel Gammon, L. J. Sham, and Duncan G. Steel, "Direct high-resolution resonant raman scattering measurements of dynamic nuclear spin polarization states of an inas quantum dot," Phys. Rev. B **102**, 235425 (2020).
[52] A. Greilich, D. R. Yakovlev, A. Shabaev, Al. L. Efros, I. A. Yugova, R. Oulton, V. Stavarache, D. Reuter, A. Wieck, and M. Bayer, "Mode locking of electron spin coherences in singly charged quantum dots," Science **313**, 341–345 (2006).
[53] A. Greilich, A. Shabaev, D. R. Yakovlev, Al. L. Efros, I. A. Yugova, D. Reuter, A. D. Wieck, and M. Bayer, "Nuclei-induced frequency focusing of electron spin coherence," Science **317**, 1896–1899 (2007).
[54] E. Evers, N. E. Kopteva, I. A. Yugova, D. R. Yakovlev, M. Bayer, and A. Greilich, "Suppression of nuclear spin fluctuations in an ensemble of (In,Ga)As/GaAs quantum dots excited with a GHz-pulsed laser," (2020), arXiv:2011.06869 [cond-mat.mes-hall].
[55] E. Evers, N. E. Kopteva, I. A. Yugova, D. R. Yakovlev, M. Bayer, and A. Greilich, "Shielding of external magnetic field by dynamic nuclear polarization in (In,Ga)As quantum dots," (2021), arXiv:2101.04469 [cond-mat.mes-hall].
[56] S. G. Carter, A. Shabaev, Sophia E. Economou, T. A. Kennedy, A. S. Bracker, and T. L. Reinecke, "Directing nuclear spin flips in InAs quantum dots using detuned optical pulse trains," Phys. Rev. Lett. **102**, 167403 (2009).
[57] S. Varwig, A. René, A. Greilich, D. R. Yakovlev, D. Reuter, A. D. Wieck, and M. Bayer, "Temperature dependence of hole spin coherence in (In, Ga)As quantum dots measured by mode-locking and echo techniques," Phys. Rev. B **87**, 115307 (2013).
[58] S. Varwig, A. Schwan, D. Barmscheid, C. Müller, A. Greilich, I. A. Yugova, D. R. Yakovlev, D. Reuter, A. D. Wieck, and M. Bayer, "Hole spin precession in a (In, Ga)As quantum dot ensemble: From resonant spin amplification to spin mode locking," Phys. Rev. B **86**, 075321 (2012).

[59] S. Varwig, A. Greilich, D. R. Yakovlev, and M. Bayer, "Spin mode locking in quantum dots revisited," physica status solidi (b) **251**, 1892–1911 (2014).

[60] Xiaodong Xu, Wang Yao, Bo Sun, Duncan Steel, Allan Bracker, Daniel Gammon, and L Sham, "Optically controlled locking of the nuclear field via coherent dark state spectroscopy," Nature **459**, 1105–9 (2009).

[61] A. S. Bracker, E. A. Stinaff, D. Gammon, M. E. Ware, J. G. Tischler, A. Shabaev, Al. L. Efros, D. Park, D. Gershoni, V. L. Korenev, and I. A. Merkulov, "Optical pumping of the electronic and nuclear spin of single charge-tunable quantum dots," Phys. Rev. Lett. **94**, 047402 (2005).

[62] C. Latta, A. Hgele, Y. Zhao, A. N. Vamivakas, P. Maletinsky, M. Kroner, J. Dreiser, I. Carusotto, A. Badolato, D. Schuh, and et al., "Confluence of resonant laser excitation and bidirectional quantum-dot nuclear-spin polarization," Nature Physics **5**, 758763 (2009).

[63] A. Högele, M. Kroner, C. Latta, M. Claassen, I. Carusotto, C. Bulutay, and A. Imamoglu, "Dynamic nuclear spin polarization in the resonant laser excitation of an InGaAs quantum dot," Phys. Rev. Lett. **108**, 197403 (2012).

[64] Michael J. Dominguez, Joseph R. Iafrate, and Vanessa Sih, "Dynamic nuclear polarization by optical stark effect in periodically pumped gallium arsenide," Phys. Rev. B **101**, 205203 (2020).

[65] Sandra Foletti, Hendrik Bluhm, Diana Mahalu, Vladimir Umansky, and Amir Yacoby, "Universal quantum control of two-electron spin quantum bits using dynamic nuclear polarization," Nature Physics **5**, 903908 (2009).

[66] D. J. Reilly, J. M. Taylor, J. R. Petta, C. M. Marcus, M. P. Hanson, and A. C. Gossard, "Suppressing spin qubit dephasing by nuclear state preparation," Science **321**, 817821 (2008).

[67] Hendrik Bluhm, Sandra Foletti, Diana Mahalu, Vladimir Umansky, and Amir Yacoby, "Enhancing the coherence of a spin qubit by operating it as a feedback loop that controls its nuclear spin bath," Phys. Rev. Lett. **105**, 216803 (2010).

[68] John Nichol, Lucas Orona, Shannon Harvey, Saeed Fallahi, Geoffrey Gardner, M. J. Manfra, and Amir Yacoby, "High-fidelity entangling gate for double-quantum-dot spin qubits," npj Quantum Information **3** (2016), 10.1038/s41534-016-0003-1.

[69] V. S. Pribiag, S. Nadj-Perge, S. M. Frolov, J. W. G. van den Berg, I. van Weperen, S. R. Plissard, E. P. A. M. Bakkers, and L. P. Kouwenhoven, "Electrical control of single hole spins in nanowire quantum dots," Nature Nanotechnology **8**, 170174 (2013).

[70] Jifa Tian, Seokmin Hong, Ireneusz Miotkowski, Supriyo Datta, and Yong P. Chen, "Observation of current-induced, long-lived persistent spin polarization in a topological insulator: A rechargeable spin battery," Science Advances **3** (2017), 10.1126/sciadv.1602531.

[71] Ewa Rej, Torsten Gaebel, Thomas Boele, David Waddington, and David Reilly, "Hyperpolarized nanodiamond with long spin relaxation times," Nature Communications **6** (2015), 10.1038/ncomms9459.

[72] Edwin Barnes and Sophia E. Economou, "Electron-nuclear dynamics in a quantum dot under nonunitary electron control," Phys. Rev. Lett. **107**, 047601 (2011).

[73] Sophia E. Economou and Edwin Barnes, "Theory of dynamic nuclear polarization and feedback in quantum dots," Phys. Rev. B **89**, 165301 (2014).

[74] Wen Yang and L. J. Sham, "General theory of feedback control of a nuclear spin ensemble in quantum dots," Phys. Rev. B **88**, 235304 (2013).

[75] Peter Stano and Daniel Loss, "Nmr response of nuclear-spin helix in quantum wires with hyperfine and spin-orbit interaction," Phys. Rev. B **90**, 195312 (2014).

[76] Thomas Nutz, Edwin Barnes, and Sophia E. Economou, "Solvable quantum model of dynamic nuclear polarization in optically driven quantum dots," Phys. Rev. B **99**, 035439 (2019).

[77] Girish Sharma, Sophia E. Economou, and Edwin Barnes, "Interplay of valley polarization and dynamic nuclear polarization in 2d transition metal dichalcogenides," Phys. Rev. B **96**, 125201 (2017).

[78] Girish Sharma, Torsten Gaebel, Ewa Rej, David J. Reilly, Sophia E. Economou, and Edwin Barnes, "Enhancement of nuclear spin coherence times by driving dynamic nuclear polarization at defect centers in solids," Phys. Rev. B **99**, 205423 (2019).

[79] Izhar Neder, Mark S. Rudner, Hendrik Bluhm, Sandra Foletti, Bertrand I. Halperin, and Amir Yacoby, "Semiclassical model for the dephasing of a two-electron spin qubit coupled to a coherently evolving nuclear spin bath," Phys. Rev. B **84**, 035441 (2011).

[80] Izhar Neder, Mark S. Rudner, and Bertrand I. Halperin, "Theory of coherent dynamic nuclear polarization in quantum dots," Phys. Rev. B **89**, 085403 (2014).

[81] M. S. Rudner and L. S. Levitov, "Self-polarization and dynamical cooling of nuclear spins in double quantum dots," Phys. Rev. Lett. **99**, 036602 (2007).

[82] J. Danon, I. T. Vink, F. H. L. Koppens, K. C. Nowack, L. M. K. Vandersypen, and Yu. V. Nazarov, "Multiple nuclear polarization states in a double quantum dot," Phys. Rev. Lett. **103**, 046601 (2009).

[83] R. Oulton, A. Greilich, S. Yu. Verbin, R. V. Cherbunin, T. Auer, D. R. Yakovlev, M. Bayer, I. A. Merkulov, V. Stavarache, D. Reuter, and A. D. Wieck, "Subsecond spin relaxation times in quantum dots at zero applied magnetic field due to a strong electron-nuclear interaction," Phys. Rev. Lett. **98**, 107401 (2007).

[84] Ceyhun Bulutay, "Quadrupolar spectra of nuclear spins in strained $In_xGa_{1-x}As$ quantum dots," Phys. Rev. B **85**, 115313 (2012).

[85] A. E. Nikolaenko, E. A. Chekhovich, M. N. Makhonin, I. W. Drouzas, A. B. Van'kov, J. Skiba-Szymanska, M. S. Skolnick, P. Senellart, D. Martrou, A. Lemaître, and A. I. Tartakovskii, "Suppression of nuclear spin diffusion at a $GaAs/Al_xGa_{1-x}As$ interface measured with a single quantum-dot nanoprobe," Phys. Rev. B **79**, 081303 (2009).

[86] E. A. Chekhovich, M. N. Makhonin, J. Skiba-Szymanska, A. B. Krysa, V. D. Kulakovskii, M. S. Skolnick, and A. I. Tartakovskii, "Dynamics of optically induced nuclear spin polarization in individual $InP/Ga_xIn_{1-x}P$ quantum dots," Phys. Rev. B **81**, 245308 (2010).

[87] Christian Latta, Ajit Srivastava, and Atac Imamoğlu, "Hyperfine interaction-dominated dynamics of nuclear spins in self-assembled InGaAs quantum dots," Phys. Rev. Lett. **107**, 167401 (2011).

[88] Wen Yang and L. J. Sham, "Collective nuclear stabiliza-

tion in single quantum dots by noncollinear hyperfine interaction," Physical Review B **85** (2012), 10.1103/physrevb.85.235319.

[89] J. M. Taylor, A. Imamoglu, and M. D. Lukin, "Controlling a mesoscopic spin environment by quantum bit manipulation," Phys. Rev. Lett. **91**, 246802 (2003).

[90] Emil V. Denning, Dorian A. Gangloff, Mete Atatüre, Jesper Mørk, and Claire Le Gall, "Collective quantum memory activated by a driven central spin," Phys. Rev. Lett. **123**, 140502 (2019).

[91] D. A. Gangloff, G. Éthier-Majcher, C. Lang, E. V. Denning, J. H. Bodey, D. M. Jackson, E. Clarke, M. Hugues, C. Le Gall, and M. Atatüre, "Quantum interface of an electron and a nuclear ensemble," Science **364**, 62–66 (2019).

[92] Daniel M. Jackson, Dorian A. Gangloff, Jonathan H. Bodey, Leon Zaporski, Clara Bachorz, Edmund Clarke, Maxime Hugues, Claire Le Gall, and Mete Atatre, "Quantum sensing of a coherent single spin excitation in a nuclear ensemble," (2020), arXiv:2008.09541 [quant-ph].

[93] Jeroen Danon and Yuli V. Nazarov, "Nuclear tuning and detuning of the electron spin resonance in a quantum dot: Theoretical consideration," Phys. Rev. Lett. **100**, 056603 (2008).

[94] M. M. Glazov, I. A. Yugova, and Al. L. Efros, "Electron spin synchronization induced by optical nuclear magnetic resonance feedback," Phys. Rev. B **85**, 041303 (2012).

[95] M. Yu. Petrov and S. V. Yakovlev, "Comparison of quantum-mechanical and semiclassical approaches for an analysis of spin dynamics in quantum dots," Journal of Experimental and Theoretical Physics **115**, 326–336 (2012).

[96] Natalie Jäschke, Andreas Fischer, Eiko Evers, Vasilii V. Belykh, Alex Greilich, Manfred Bayer, and Frithjof B. Anders, "Nonequilibrium nuclear spin distribution function in quantum dots subject to periodic pulses," Phys. Rev. B **96**, 205419 (2017).

[97] Iris Kleinjohann, Eiko Evers, Philipp Schering, Alex Greilich, Götz S. Uhrig, Manfred Bayer, and Frithjof B. Anders, "Magnetic field dependence of the electron spin revival amplitude in periodically pulsed quantum dots," Phys. Rev. B **98**, 155318 (2018).

[98] Philipp Schering, Jan Hüdepohl, Götz S. Uhrig, and Benedikt Fauseweh, "Nuclear frequency focusing in periodically pulsed semiconductor quantum dots described by infinite classical central spin models," Phys. Rev. B **98**, 024305 (2018).

[99] Philipp Schering, Götz S. Uhrig, and Dmitry S. Smirnov, "Spin inertia and polarization recovery in quantum dots: Role of pumping strength and resonant spin amplification," Phys. Rev. Research **1**, 033189 (2019).

[100] Philipp Schering, Philipp W. Scherer, and Götz S. Uhrig, "Interplay of spin mode locking and nuclei-induced frequency focusing in quantum dots," Phys. Rev. B **102**, 115301 (2020).

[101] Daniel Stanek, Carsten Raas, and Götz S. Uhrig, "Dynamics and decoherence in the central spin model in the low-field limit," Phys. Rev. B **88**, 155305 (2013).

[102] Daniel Stanek, Carsten Raas, and Götz S. Uhrig, "From quantum-mechanical to classical dynamics in the central-spin model," Phys. Rev. B **90**, 064301 (2014).

[103] Tomasz Dietl, "Spin dynamics of a confined electron interacting with magnetic or nuclear spins: A semiclassical approach," Phys. Rev. B **91**, 125204 (2015).

[104] S. G. Carter, Sophia E. Economou, A. Shabaev, and A. S. Bracker, "Controlling the nuclear polarization in quantum dots using optical pulse shape with a modest bandwidth," Phys. Rev. B **83**, 115325 (2011).

[105] Edwin Barnes, Łukasz Cywiński, and S. Das Sarma, "Nonperturbative master equation solution of central spin dephasing dynamics," Phys. Rev. Lett. **109**, 140403 (2012).

[106] Edwin Barnes, Łukasz Cywiński, and S. Das Sarma, "Master equation approach to the central spin decoherence problem: Uniform coupling model and role of projection operators," Phys. Rev. B **84**, 155315 (2011).

[107] A. Abragam, *The Principles of Nuclear Magnetism*, The international series of monographs on physics (Clarendon Press, 1970).

[108] C. P. Slichter, *Principles of Magnetic Resonance*, Springer Series in Solid-State Sciences (Springer Berlin Heidelberg, 1996).

[109] Michael A. Nielsen and Isaac L. Chuang, *Quantum Computation and Quantum Information: 10th Anniversary Edition* (Cambridge University Press, 2010).

[110] Thomas F. Jordan and E. C. G. Sudarshan, "Dynamical mappings of density operators in quantum mechanics," Journal of Mathematical Physics **2**, 772–775 (1961).

[111] Thomas F. Jordan, Anil Shaji, and E. C. G. Sudarshan, "Dynamics of initially entangled open quantum systems," Phys. Rev. A **70**, 052110 (2004).

[112] Albert W. Overhauser, "Polarization of nuclei in metals," Phys. Rev. **92**, 411–415 (1953).

[113] W. D. Knight, "Nuclear magnetic resonance shift in metals," Phys. Rev. **76**, 1259–1260 (1949).

[114] W. M. Witzel and S. Das Sarma, "Quantum theory for electron spin decoherence induced by nuclear spin dynamics in semiconductor quantum computer architectures: Spectral diffusion of localized electron spins in the nuclear solid-state environment," Phys. Rev. B **74**, 035322 (2006).